Chapter 6

Catastrophic mass failure of a Middle Cambrian platform margin, the Lawn Hill Megabreccia, Queensland, Australia

Acknowledgement of Contributions

N.H.S. Oliver – normal supervisory contributions

Abstract

Megabreccia and related folds are two of the most spectacular features of the Lawn Hill Outlier, a small carbonate platform of Middle Cambrian age, situated in the northeastern part of the Georgina Basin, Australia. The megabreccia is a thick unit (over 200 m) composed of chaotic structures and containing matrix-supported clasts up to 260 m across. The breccia also influenced a Mesoproterozoic basement, which hosts the world class Zn-Pb-Ag Century Deposit. Field-studies (undertaken in the mine area), structural 3D modelling and stable isotopic data were used to assess the origin and timing of the megabreccia, and its relationship to the tectonic framework. Previous workers proposed the possible linkage of the structural disruption to an asteroid impact, to justify the extremely large clasts and the conspicuous basement interaction. However, the megabreccia has comparable clast size to some of the largest examples of sedimentary breccias and synsedimentary dyke intrusions in the world.

Together with our field and isotope data, the reconstruction of the sequence of events that led to the cratonization of the Centralian Superbasin supports a synsedimentary origin for the Lawn Hill Megabreccia. However, later brittle faulting and veining accompanying strain localisation within the Thorntonia Limestones may represent post-sedimentary, syntectonic deformation, possibly linked to the late Devonian Alice Springs Orogeny. An origin linked to an asteroid impact cannot be completely discounted, but the coupling of intrabasinal processes involving destabilization along the platform margin associated with diagenetic karstification and

tectonic dip-slip reactivation of basement faults, explain adequately the documented features.

Keywords: Lawn Hill Outlier, Megabreccia, Century, Dykes, Debris-Flow, Slumps

6.1 Introduction

Understanding the origin and timing of catastrophic events is of primary importance for earth scientists and modern urban society. Modern technologies have the potential to allow identification of early signs of massive failure (e.g. aseismic fault slip on the flank of volcanoes, Cervelli et al., 2002), but the multivariate nature of geological systems still requires the acquisition of data across different geological terrains and time periods, to understand the interplay of variables (such as faulting, lithostratigraphy, climatic conditions, etc.) leading to these "rare" events. Catastrophic sedimentary processes may occur either in continental or marine settings, as a result of intrabasinal evolution or extra-basinal forcing mechanisms (Rossetti et al., 2003), reflecting the nonlinear behaviour of the earth crust (see Nicolis, 1995). Important external causative factors are seismogenic events, either earthquakes or tsunami, but also aseismic events such as meteorite impacts, or hurricanes (Albertao et al., 1996; Shiki et al., 2000). Here we present a case study of a "catastrophic" event that led to the formation of one of the largest breccia accumulations in the world, the Lawn Hill Megabreccia.

Defining the timing and origin of catastrophic events is valuable also for tecnostratigraphic reconstructions, because these deformations can be potentially caused by tectonic movements. For instance, the Lawn Hill Outlier may have been deformed by the Late Devonian, Alice Springs Orogeny (ca. 410-390 Ma), which influenced other Palaeozoic basins in central and northern Australia (e.g. Haines et al., 2001). Therefore, a detailed structural and stratigraphic analysis was undertaken to assess the possible influence of such an orogenic event. A review of the tectonic framework and stratigraphic evolution of the Georgina Basin is presented below and the timing and origin of folding, brecciation and dyke intrusions into the underlying Mesoproterozoic basement is discussed.

The megabreccia is hosted in the Lawn Hill Outlier (originally named as Dentalium Plateaux, Carter and Opik, 1961), located approximately 250 km north northwest of Mount Isa in Queensland (Fig. 6.1a-c). The Outlier has a circular shape, with diameter of 18 km, and unconformably overlays Mesoproterozoic weakly metamorphosed rocks of the Mount Isa Inlier (mainly siltstones and shales of the McNamara Group, Andrews, 1998). The Outlier was firstly mapped by Opik (1957) who used biostratigraphic correlations to define its Middle Cambrian age, and included the carbonate rocks as part of the Thorntonia Limestone, Beetle Creek and Border Waterhole Formations of the Georgina Basin. The Lawn Hill Outlier overlies, on its southwestern margin, one of the largest Zn-Pb-Ag mineral deposits in the world, the Century zinc deposit. This mineral resource is currently mined in open cut by Zinifex Pty Ltd. offering a unique chance of studying large exposures (approx. 250 m high) that represent sections throughout the sedimentary sequence of the Thorntonia Limestone.

The open cut also exposes an erosional unconformity that separates the Mesoproterozoic strata of the Lawn Hill Formation (e.g. Andrews, 1998) from the carbonate cover sediments of the Georgina Basin.

The anomalous folding and brecciation of the Lawn Hill Outlier have been interpreted in diverse ways. De Keyser (1969) invoked dip-slip reactivation of Mesoproterozoic basement faults as the mechanism controlling the formation of the megabreccia. Other workers suggested an early Middle Cambrian asteroid impact as a possible explanation for the complex brecciation and folding observed, and the circular outcrop pattern (Ferguson, 1992). In contrast to De Keyser (1969), Hutton (1992) explained the deformation by solution collapse in limestones elsewhere in the basin. Hutton (1992) also discounted the possibility of a connection between deformational features and an extraterrestrial impact, suggesting that occurrence of cone in cone structures in the central part of the outlier could be also derived by simple volcanic, explosive activity. In summary, several processes operated independently or interactively to cause the observed deformational features and these include: (1) tectonic control with possible reactivation of basement structures; (2) asteroid impact; (3) solution collapse due to karstic activity.

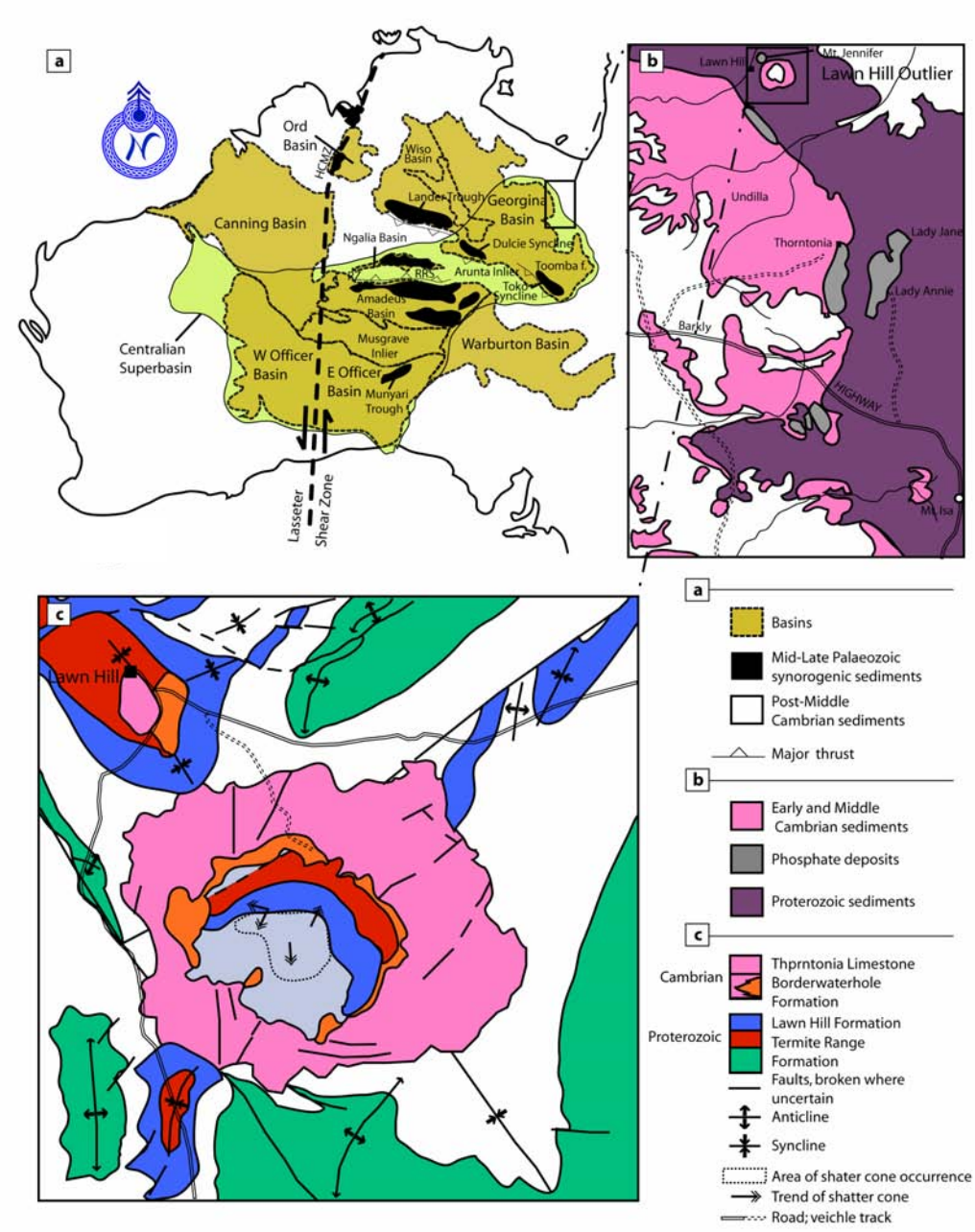

Fig. 6.1 Map view of the study area: (a) locality map (after, Haines et al., 2001) showing main basins (Amadeus, Ngalia, Georgina, Officer, and Savory) and inliers discussed in the text. Delimitation of the Centralian Superbasin and location of Dulcie and Toko synclines. (b) Locality map showing the northeastern margin of the Georgina Basin (Undilla sub-Basin) and location of the Lawn Hill Outlier. (c) Enlarged map-view of the Lawn Hill Outlier illustrating the lithofacies variation in the study area, and the distribution and trends of shatter cones (after Stewart and Mitchell, 1987).

6.2 Regional geotectonic framework

The tectonostratigraphic evolution of the Centralian Superbasin provides elements at cratonic/regional scale that can be used to spatially and temporally define the Lawn Hill Megabreccia event, relative to major tectonic events.

6.2.1 From intracratonic to orogenic times

The Lawn Hill Outlier is formally correlated with the northeastern margin of the Georgina Basin (Undilla sub-Basin) based on lithostratigraphic and biostratigraphic correlations (Szulc, 1992). The Georgina Basin is one of five sedimentary compartments (e.g. Walter et al., 1995) that resulted from the Neoproterozoic separation of an extensive (approx. 2 million km^2) intracratonic basin, termed the Centralian Superbasin (Gorter, 1992; Walter et al., 1992; Walter et al., 1995) (Fig. 6.1a). This Superbasin underwent an initial phase of intracratonic rifting that culminated with Early Cambrian seafloor spreading accompanied by subsidence and crustal thinning at around 800 Ma (Shaw et al., 1991; Zhao et al., 1994). Sub-basins were apparently preserved where little Neoproterozoic and Palaeozoic orogenic deformation occurred (Walter et al., 1995; Sandiford and Hand, 1998). However, the history of sedimentation of basin compartments may have been influenced by these major tectonic events. Understanding how the deformation evolved at cratonic to regional scale, and when such phases developed is essential when attempting to define the origin and timing of brittle and ductile deformation observed at the local scale.

Two orogenies have contributed to the separation of the Centralian Superbasin, with consequent uplifting and exposure of two high-grade metamorphic complexes, the Arunta and Musgrave Inliers (Fig. 6.1a). The oldest event is the Petermann Orogeny (Early Cambrian, ca. 540-600 Ma) is linked to the exhumation of the Musgrave Inlier involving northward-directed thrusting over the southern margin of the Amadeus basin. The younger Alice Springs Orogeny (ca. 410-390 Ma) was involved with the Arunta Inlier uplift causing southward-directed thrusting, thereby separating the Amadeus Basin, on its southern margin, from the northern Georgina Basin (e.g. Walter et al., 1995; Sandiford and Hand, 1998). Although the Petermann and Alice Springs Orogenies are separated by a minimum of 150 Ma they share similar characters. For instance, the shear zones that acted within the metamorphic core generally trend E-W, dipping toward the hinterland. Throughout the evolution of the Centralian Superbasin, depocentres shifted producing localised, sedimentary compartments with thick piles of sediments. Hand and Sandiford (1999) proposed that early sedimentary thickening, accompanied by thermal weakening and synsedimentary faulting, represents the required precursor to orogenesis, causing its localisation. This mechanism was also inferred to be responsible for the reactivation of Proterozoic basement faults (Glickson et al., 1995; Glickson et al., 1996; Hand and Sandiford, 1999) during basin inversion (e.g. within the Redbank Thrust Zone, Korsch et al., 1998). In this context, the thick accumulations (3 - 10 km of maximum stratigraphic thickness) of sedimentary fill observed in the southern margin of the Georgian Basin (Dulcie and Toko Synclines, see Fig. 6.1a), may have been part of pre-orogenic thick domains responsible for the subsequent localisation of the Late Devonian (ca. 410-390 Ma) Alice Springs Orogeny.

The orogenic overprint seems then to be fairly restricted to the southern margin of the Georgina Basin. Sedimentation here started earlier than the Petermann Orogeny and continued till post-Alice Springs Orogeny time (Fig. 6.2). Orogenic deformation acted upon the Georgina Basin in a twofold manner, influencing either its sedimentation or subdividing and folding the strata. In the southern margin of the basin the Toko and Dulcie synclines record this tectonic overprint. These structures are northwest – southeast trending folds with their steep limbs in contact with the metamorphic rocks of the Arunta Inlier. Haines et al. (2001) remark that sedimentary deposition, within the synclines, is locally coarser and conglomeratic (e.g. Cravens Peak beds and Dulcie Sandstone) (Fig. 6.2), providing possible indication of a non-marine setting due to orogenic uplift. The workers also suggest that local folding may have originated during sedimentation, but a synorogenic component may have contributed to its formation. There is finally evidence within the synclines of faults that have close connection with the thrusting observed in the Arunta Inlier (Haines et al., 2001).

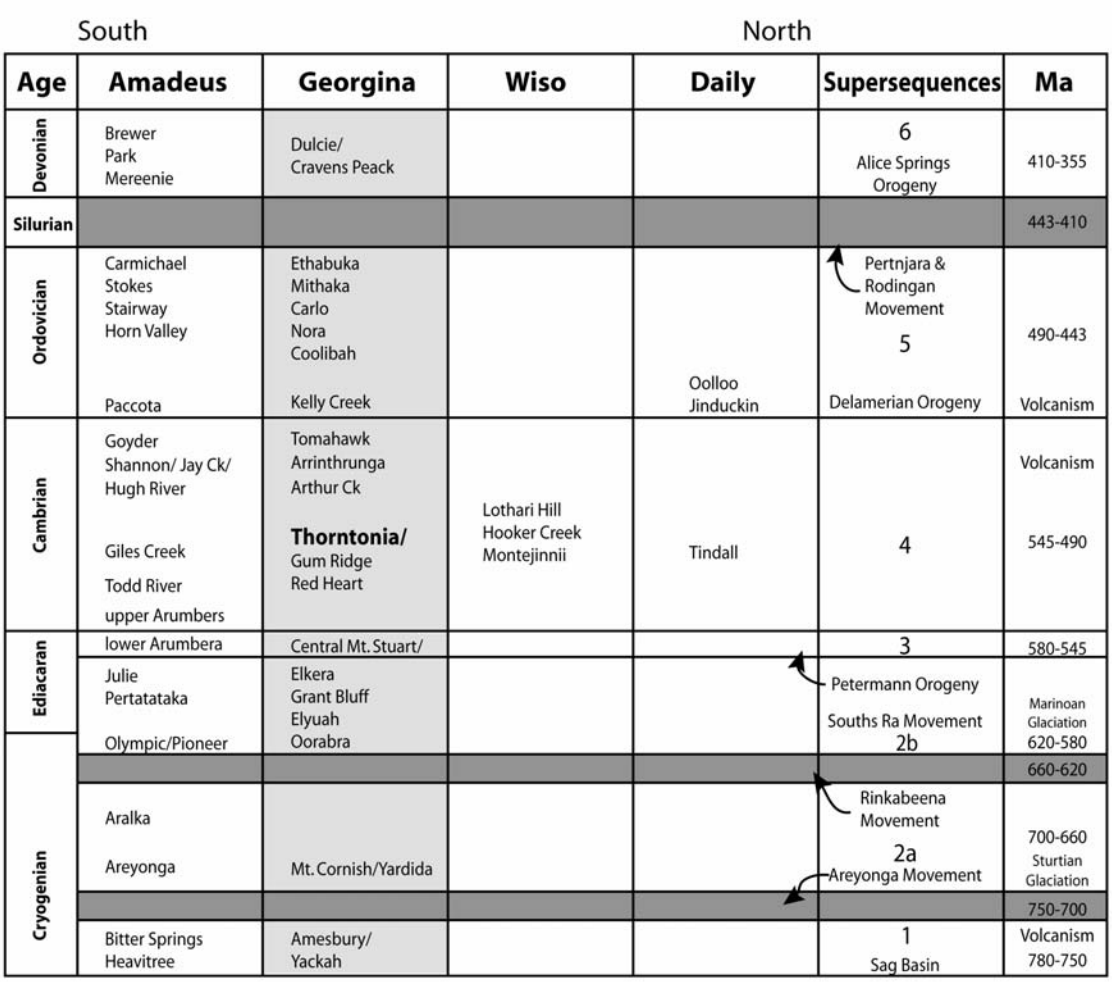

Fig. 6.2 Simplified stratigraphy from south to north through the Amadeus, Georgina, Wiso and Daly Basins (redrawn from Lindsay et al., 2005).

Although the Lawn Hill Region was relatively far from these sites of intense deformation, Sandiford and Hand (1998) remark that the Alice Springs Orogeny acted on an extensive part of the Amadeus basin (see Fig. 6.1a) to the south, causing overprinting of Petermann Orogeny folds that were tightened by coaxial N-S shortening. The effect of contractional deformation during the orogen extended for more than 200 km outward from the metamorphic core (Fig. 6.3a, b). Perhaps a similar

extent of orogenic overprinting occurred above the northern margin the Arunta Inlier and contributed to faulting and folding of Middle Cambrian sediments in the Georgina Basin. Hand and Sandiford (1999) report that north of the Arunta Block the basement was thrust northward over Neoproterozoic and early Palaeozoic cover sequences of the Georgina and Wiso Basins (Fig. 6.3a, b). These authors also suggest that the thrusts developed on pre-existing syn-rift faults, contributed to their reactivation. N-S verging orogens had the ability to reactivate predominantly E-W trending basement faults, a case that could be valid also for the E-W basement structures occurring in the study area.

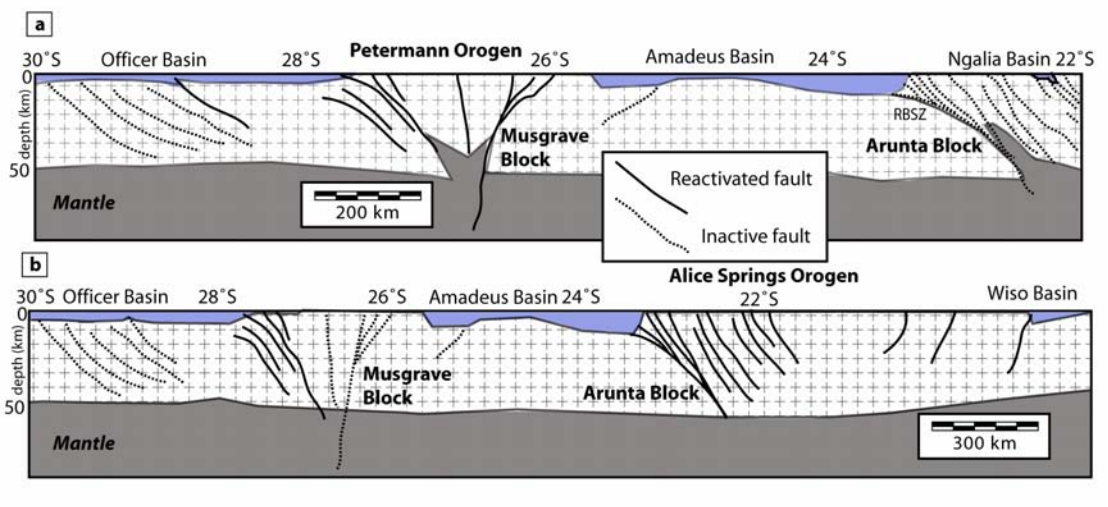

Fig. 6.3 Crustal transect (after Korsch et al., 1998) showing the locus of reactivation during the Petermann and Alice Springs Orogenies. Note the reactivation of basement, south dipping faults during Alice Springs Orogeny proximal to the Wiso Basin. Other structures at similar distance from the core of the orogen may have been reactivated in a similar way within the adjacent Georgina Basin (adapted from Hand and Sandiford, 1999). RBSZ = Redbank Shear Zone.

Scattered examples of possible tectonic related deformation have been reported for the northern part of the Georgina Basin. However, local examples of folding and

faulting may have an origin that is unrelated to the Alice Springs Orogeny and could be for example due to gravity driven deformation – this would be justifying their fairly localised occurrence. For instance, Smith (1972) reports the existence of a structural belt on the southeastern margin of the Georgina Basin in Queensland. Evidence of asymmetric folds is reported also in the Neoproterozoic and Cambrian Outliers found in the Mount Isa and McArthur Basins, such as the one considered in this study (Lawn Hill Outlier) or in the Abner Range of the McArthur Basin, where the late Neoproterozoic to Cambrian Bukalara sandstone appears to be folded with northwest orientation (Jackson et al., 1987; Pietsch et al., 1991; Haines et al., 2001). A preliminary conclusion could be then that the Alice Springs orogenic overprint might have been sufficient in the Lawn Hill Region to cause reactivation of faults and folding of Middle Cambrian sediments although a careful assessment of the style of deformation is required, because anorogenic deformation may produce similar patterns (e.g. van Loon, 2003).

6.2.2 Stratigraphic evolution of the Centralian Superbasin

A brief examination of the sedimentary evolution of the Centralian Superbasin is reviewed here, to place the Georgina Basin into its tectonostratigraphic context. The time interval between 800 and 355 Ma can be formally subdivided into six main supersequences (Fig. 6.2) (Walter et al., 1995; Lindsay et al., 2005). Supersequence 1, (lower Cryogenian) initiated with massive deposition of sandy intervals that are thicker

to the west in the Savory Basin (Bitter Springs, Heavitree Formations - Amadeus Basin) and Yackah beds and Amesbury Formation - Georgina Basin). A sharp variation in the lithofacies sealed the top of Supersequence 1 and is characterised by more marine to lacustrine sequences, predominantly carbonates, evaporates and fine siliciclastics. Supersequence 2 (upper Cryogenian-lower Ediacaran) has a similar succession on its top part, with carbonates and shales, but it is distinct for its basal (Sturtian, ca. 660-650 Ma) glacigene sediments. Supersequence 3 also has glacial sediments at its base (Marinoan, ca. 600-610 Ma), followed by a widespread transgression with deposition of turbiditic sandstones and shales. Carbonates and evaporates cap the sequence. The Phanerozoic sedimentation starts with extensive deposition of sandstones and silts (Supersequence 4 - Lower Cambrian), accompanied by eruption of continental flood basalts that terminated with the final stages of the Petermann Ranges Orogeny (ca. 540 Ma ago). The younger, transitional part of the sequence (lower part of Supersequence 4) is dominated by initial siliciclastic deposition of sandstones and silts characteristic for the presence of "Ediacara fauna" that is however poorly represented within the Centralian Superbasin (Walter et al., 1995). This is then followed by shallower depositional settings with abundant carbonates and evaporites indicative of arid climates (e.g. Thorntonia Limestone in the Georgina Basin, upper part of Supersequence 4). Supersequence 5 (Ordovician) is characterised by an initial marine sedimentation of sandstone and siltstones represented by the Larapinta Group in the Amadeus Basin, which terminates with the Stokes siltstone (Shergold et al., 1991) and is equivalent to the Mithaka Formation and underlying sequences in the Georgina Basin. A permanent change in the style of sedimentation (with a more fluvial

component) occurred then with the incoming of coarse clastic sediments. These form the base of the Carmichael Sandstone in the Amadeus Basin and are correlated to the youngest Ordovician interval in the Georgina Basin, the Ethabuka Sandstone (Shergold et al., 1991; Haines et al., 2001). Supersequence 6 is distinct by the onset of the Alice Springs Orogeny that provides coarser, clastic fills, derived from uplift and erosion, to the surrounding basins. This phase of uplift is contemporaneous with the deposition of the Mereenie Sandstone, derived from aeolian and fluvial environments in the Amadeus Basin; whereas in the Georgina Basin post-Ordovician, non-marine sequences were deposited in the Toko and Dulcie synclines. These are mainly pebbly to boulder conglomerates (Cravens Peak beds) that locally are found also in the Dulcie Sandstones. The effect of the Alice Springs Orogeny is more intense in the late Devonian with coarsening upward deposition of the Pertnjara Group (Haines et al., 2001). The group is preserved locally near the northern margin of the Amadeus Basin and comprises fluvial and aeolian sandstones.

Climatic conditions as seen can contribute significantly to massive failure events. For instance, abundant rainfall may cause instability of land masses or rock falls may occur in response to tidal variation along a platform margin. It is therefore important to establish the climatic context in which a “catastrophic event” has taken place to ascertain its origin. The reviewed stratigraphic evolution provides an indirect way to assess the climatic change, and suggests that an initial phase of relatively cold climates is progressively superseded by wormer sub-tropical conditions that culminated with the Cambrian faunal explosion. Beside the biological implications of seawater temperature

variations these considerations therefore exclude a possible relationship of the Lawn Hill Megabreccia to glacial processes (e.g. Arnaud and Eyles, 2002).

6.3 Georgina Basin

A more focused description of the Georgina Basin is now presented, with further detail of the stratigraphic record relative to the Undilla sub-Basin, to better constrain the location of the Lawn Hill Outlier and its stratigraphic context. The time of deposition of carbonates forming the outlier is also reviewed considering its fossil content, to provide an understanding of the biostratigraphic framework, which is important for later considerations on the origin and timing of deformational features.

6.3.1 Introduction

The Georgina Basin is characterised by variable thicknesses that rarely exceeds 3 km. Mostly flat laying strata extends for approximately 325,000 km^2 across northern Queensland and the eastern part of the Northern Territory (Shergold and Druce, 1980) (Fig. 6.1a, b). Sedimentary rocks of the Georgina Basin cover a predominantly Palaeo- to Mesoproterozoic basement. The sediment fill varies from west to east with a gradual shift from predominantly siliciclastic to more carbonate-rich components (Shergold et al., 1976). On its northeastern margin the basin unconformably overlies the Mesoproterozoic rocks of the Lawn Hill Platform of the Mount Isa Inlier; whereas in its southern and western part it terminates against Palaeo- to Mesoproterozoic rocks of the

Arunta and Tennant Creek Inliers (Compston, 1995; Haines et al., 2001). The Lawn Hill Outlier is situated along the northeastern margin of the Georgina Basin (Undilla sub-Basin, see Fig. 6.1b), and is characterised by Middle Cambrian sediments, predominantly carbonate and dolomites, locally evaporitic and rich in phosphorites – the latter being an important mineral resource of northern Queensland (De Keyser and Cook, 1972). Several parts of the basin were also unsuccessfully explored for petroleum reservoirs, because the fossil shales and siltstones contain significant traces of hydrocarbons (see Glikson et al., 1985). The sequence of depositional facies supports interpretations for the palaeogeographic setting that varied from marine slope, ramp dominated facies to sabhka-type, supratidal depositional settings. The palaeogeographic scenario was likely a Cambrian epeiric sea surrounded by islands formed by uplifted metamorphosed blocks and terminated against the Gondwana margin (Shergold et al., 1976).

6.3.2 Main formations Undilla sub-Basin

The Undilla Basin represents the easternmost part of the Georgina Basin and is stratigraphically correlated with the Lawn Hill Outlier. The sub-basin rarely exceeds 400 m thickness. It comprises sedimentary rocks of Lower to Middle Cambrian age. Several classifications based on lithostratigraphic and biostratigraphic subdivisions have been proposed (e.g. Opik, 1957; De Keyser, 1973; Shergold and Druce, 1980). A simplified classification using the six lithosomes of De Keyser (1973), was particularly useful during fieldwork and mapping of pit faces within the Century Mine area, which

is located on the southwestern margin of the Lawn Hill Outlier. More detailed biostratigraphic subdivisions of Opik (1957; 1958; 1970; 1975; 1982) cannot be used so confidently in outcrop. De Keyser (1973) distinguishes the rocks of the Georgina Basin as follow: (1) basal sandstone-conglomerate lithosome (deposited during an initial transgressive littoral-marine phase); (2) chert-siltstone-limestone-phosphate lithosome (deposited in extremely shallow water, on a shelf characterised by shoals and a coastline broken by embayment, estuaries, and lagoons); (3) silt-shale-chert lithosome (deposited under conditions of quiet sedimentation in slightly deeper water); (4) limestone lithosome (deposited some distance off-shore in open marine conditions); (5) dolomite lithosome (deposited in intertital mud flats, saline lagoons, and lakes); and (6) sandstone-siltstone lithosome (deposited during a regressive clastic phase).

Mapped lithosomes in the study area include the formal names of Mount Hendry Formation, Thorntonia Limestone, Beetle Creek, and Border Waterhole Formations. The Mount Hendry Formation consists of conglomerates and ferruginous, sandstone interbeds of littoral-marine and possible fluvial origin of lower Cambrian age (Smith, 1972; De Keyser, 1973). This interval has variable thickness with a maximum of approximately 25 m. The top part of this formation is dolomitic and locally grades into the Thorntonia Limestone (De Keyser, 1973). The early Middle Cambrian 509-506 Ma Thorntonia Limestone, Beetle Creek and Border Waterhole Formations are characterised by abundant transgressive deposition of cherty and dolomitic limestone. Outcrop is usually lumpy and nodular representing the residual cherty part of the cherty-carbonates. Bioclastic layers (silicified microcoquinites) are common. Carbonate strata are interleaved with clastic beds that vary from siltstone to shales. Shales and

siltstones can be distinguished for the persistent lamination and locally for the elevated fossil content. Limestones are predominantly white, cream or grey depending on their alteration and phosphate content. Within the upper part of this lithosome local dolomite-rich laminae can be found intercalated with carbonate biopelsparites (up to 2 mm) (Szulc, 1992).

The fossil content of the Cambrian limestones is diverse. De Keyser and Cook (1972) report the following fauna: trilobites (e.g. Xystridura, Redlichia, Dolichometopid, see Opik, 1958, 1970, 1975, 1982) and also Hyolithus, echinoderms, phosphatic brachiopods, sponge spicules and algal Girvenella structures. Szulc (1992) reports the occurrence of fragments of trilobites in the Lawn Hill Outlier resembling, probably, cranidia of ptychariid trilobites of the Middle Cambrian genus Asthenopsis, and thus the worker proposes a close correlation of the Lawn Hill Outlier with the northeastern margin of the Georgina Basin on the basis of lithostratigraphic correlations and documented fossil record. Biological records also constrain the age of the Thorntonia Limestone and other carbonate formations to within the early Middle Cambrian (Ordian/Templetonian ca. 506-509 Ma, see Lindsay et al., 2005). The fossils suggest relatively shallow water depositional settings (De Keyser, 1973). However, considerable transport may have influenced the present spatial location of certain lithofacies and their relative biostratigraphic record (see below).

6.3.3 Summary

The established tectonostratigraphic framework and timing of the Thorntonia Limestone sedimentation places this event between the Petermann and Alice Springs Orogeny. Approximately 70 m.y. elapsed from the onset of the Petermann Orogeny and the deposition of the limestones. Moreover, the distance of the northeastern Georgina Basin from the core of the Petermann Orogeny exceeds the 600 km. Therefore, the Petermann event probably had a negligible effect during Ordian/Templetonian sedimentation, in the Georgina Basin. In contrast, some of the deformation observed in the basin, as seen, seems to have possible relationship with the Alice Springs Orogeny. This orogeny took place during Devonian time and therefore it may have only acted upon Ordian/Templetonian rocks after their lithification. In other words, the Alice Springs Orogeny did not influence the sedimentary deposition of the Thorntonia Limestone and other coeval formations. It becomes relevant then to characterise the style of deformation in the Lawn Hill Outlier, to ascertain if the deformation occurred during synsedimentary timing (unrelated to Alice Springs Orogeny) or later syntectonic timing.

6.3.4 Folding and brecciation in the Lawn Hill Outlier

Complex overturning of strata and brecciation have been documented by previous workers in the Lawn Hill Outlier and monoclinal folding is reported for several parts of the Georgina Basin (De Keyser and Cook, 1972; Henderson and

Southgate, 1980; Andrews, 1991; Southgate and Shergold, 1991; Szulc, 1992). The following part deals with the characterisation of deformational features observed in the Lawn Hill Outlier. The main objective is to establish the timing of recumbent folding and brecciation. To explain these structural features three different models have been proposed:

- Syn-depositional soft sediment slumping (Andrews, 1991).
- Large scale dissolution of salt forming a collapse breccia (Hutton, 1992).
- Sediment fill and solution breccia inside a crater formed by asteroid impact (Stewart, 1986; Stewart and Mitchell, 1987).

Sediment slumping is only a single aspect of the deformation observed in the region and it may be caused either by failure induced by gravitational instability or in response to instability due to an asteroid impact (point three above). Breccias and folds may also form during orogenic related deformation.

Following Elliott and Williams (1988) we recognise that these styles of deformation may be caused by: (1) local shear; (2) local density gradients; (3) gravity acting on a slope (4) glacio-tectonic processes and (5) the convergence of lithospheric plates. (6) The impact of an asteroid is also considered (extraterrestrial, external to earth processes). These mechanical forces may operate either in a synsedimentary stage or after complete lithification of the sequence, post-burial and diagenesis. These are important distinctions to make because they allow the definition of the timing of deformation. However, earlier gravitational collapse could be overprinted by faulting

and fracturing related to later tectonic deformation. The examination of the style of deformation must therefore consider several time periods as well as multiple scales in order to determine the nature and scale of overprinting.

6.4 Deformational and fluidisation related features

Observed deformational features are here classified using a twofold subdivision that considers (a) ductile, (plastic) deformational features, and (b) more brittle style deformation. The former includes: (1) recumbent and nappe-style folds; (2) injection dykes (mud lime dykes), and (3) monoclinal, gentle, dome-shaped folds. Brittle fractures include: (1) megabreccia with clasts of limestone and basement strata, and (2) post-sedimentary faults and fractures, often accompanied by veins. Notice that this subdivision does not refer to a specific timeframe of the basin history.

Maltman (1984) suggests that certain features, commonly interpreted as post-sedimentary, may form earlier. This is because consolidation does not necessarily imply a completed lithification of the rock. Prior to and during early diagenesis the pore pressure variation largely controls the apparent cohesion of a certain rock-type, because the apparent cohesion is function of the % water content. This causes temporal and spatial fluctuations of the degree of material consolidation. Therefore, during a synsedimentary or diagenetic phase certain portions of the rock-mass may behave as a brittle or brittle-ductile material and undergo consequent intra-crystalline deformation (deformation bands, lamellae, twins and pressure solution), whereas others may respond plastically with intergranular movement or elastically by pore pressure movement

(poro-elasticity) (Oliver et al., 2006). Nonetheless, in the following section we attempt to make a distinction between soft-sediment and hard-rock deformation to constrain its age. This approach can be improved using multiple datasets rather than focussing on a single distinctive element. The discussion aims to integrate the detailed observations and structural analyses and determine the timing these features.

6.4.1 Folding

6.4.1.1 General description of folds:

Pit exposures display a range of fold patterns. Overturned folds range in scale from a few centimetres to hundreds of metres (Figs. 6.4a, b and 6.5a-d). Several folds are tight, and some are isoclinal, and are either cylindrical or non-cylindrical. Notably there is a rapid spatial variation from relatively chaotic breccias through to more complexly folded areas (Fig. 6.4b). On the eastern and northern walls sub-horizontal to low-angle dipping erosional/depositional scars are present (Figs. 6.4a, b and 6.6a). Locally injected marl dykes are observed proximal to and along the scar discontinuities (Fig. 6.6b, c).

6.4.1.2 Folding patterns

Folding patterns have been often discussed at length in the literature trying to address their timing and origin (e.g. Williams et al., 1969; Helwig, 1970; Blatt et al., 1980; Elliott and Williams, 1988; Smith, 2000). However, it has been demonstrated that geometries typical of unlithified rocks develop also in lithified sediments (Elliott and Williams, 1988).

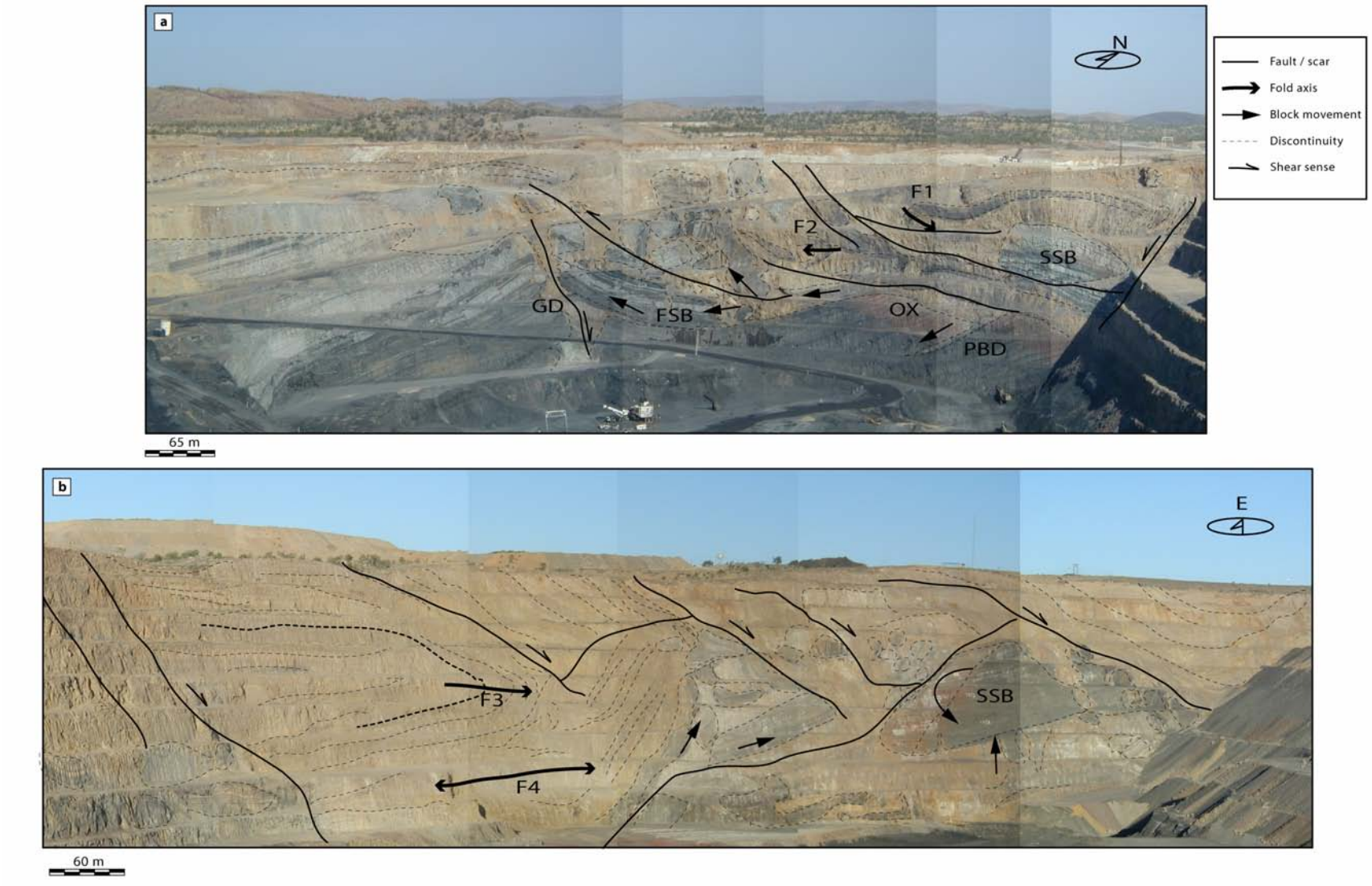
a
N
Fault / scar
Fold axis
Block movement
Discontinuity
Shear sense
F1
F2
SSB
GD
FSB
OX
PBD
65 m
b
E
F3
F4
SSB
60 m

Fig. 6.4 Photographic view and relative structural interpretation of the northern and eastern walls of the Century Mine. (a) Northern side of the Century Mine exposing a sectional view of the Lawn Hill Megabreccia deposited on top of Mesoproterozoic basement composed of black shales, siltstones and chloritic sandstones. The complexity of mechanical interaction with the basement is outlined by several Proterozoic blocks of sandstones/siltstones entrained in the carbonate, breccia matrix (e.g. SSB). A large flat-shaped block (FSB) has been displaced for more than 50 metres in a westerly direction and is bound on its western side by the largest carbonate intrusion in basement (GD), which formed synchronously with apparent dip-slip movement of a steep dipping basement fault. Another indication of apparent extensional deformation is derived from normal displacement of the basement visible on the eastern part of (a) where the oxidised basement (OX) accommodates the deformation with bedding parallel slip accompanied by injection of carbonate slurry (PBD) along the fault boundary. Folding is represented at this scale by recumbent structures (e.g. F1 – 20/120, F2 – 5/304); note the unfolded basement below, which suggests a localisation of ductile deformation in the cover. The basement being more competent is only fractured by post-Middle Cambrian faults. (b) The eastern wall of Century mine displays the biggest recumbent fold within the mine, approximately 200m vertically (F3 – 10/208). The fold is truncated on its northern and southern margin by a set of faults and breccias with mega-clasts composed of bedded limestone. Another recumbent fold lies underneath F3 (F4 – 10/115), but displays orthogonal orientation. Variation of fold axes may have been due to local tilting during accommodation of slumps. Often folds sharply abut against floating breccia blocks.

Therefore, features such as distorted and overturned strata, thickening and thinning, striated folds or fragments, rolled up fragments, detached fold beds, curvilinear fold hinges, folded boudins and chaotic structures (not cut by open fractures or vein filling), can be used only to corroborate the hypothesis of an early (soft-sediment) deformation, if other diagnostic features are well documented. The first examples recognised in the Century area that could be interpreted as indicating soft sediment folding are intrastratal, piled up, recumbent, or nappe-like folds. According to Elliot and Williams (1988) these can be considered a diagnostic criteria only if they are confined within certain stratigraphic intervals – they have to be intrastratal (see also van Loon, 2003). This feature is documented in the North wall of the Century pit (stages 4-5, see Figs. 6.5d, 6.6a), which shows an example of intrastratal folding and brecciation overlain by flat, undeformed layers. The feature is considered diagnostic by Williams et

al. (1969) because undeformed layers on top of a complexly folded intrastratal unit would be explained easily if the top part of the sequence was sedimented after the deformational event that caused slumping and overturning.

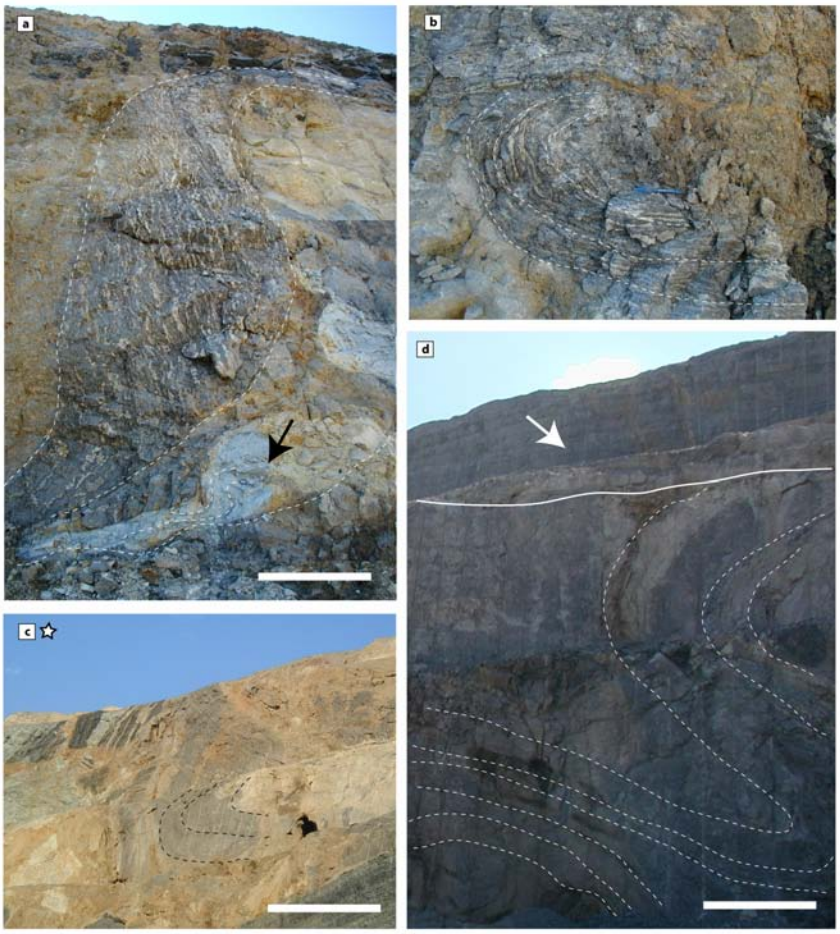

Fig. 6.5 Examples of folding patterns observed in the Thorntonia Limestone. (a) Sigmoidal folding occurring along sub-horizontal shear planes that induced reorientation of mottled, cherty limestone with characteristic parallel bedding siliceous concretions (scale bar 1.5 m). A Marl dyke (black arrow) that resulted was deformed by the same shearing event and also cross-cut by a later intrusion of CBX – the ductile response of marly layers and cherty limestones could have been contemporaneous. Nonetheless, the different phases of overprint may be derived by progressive phases of deformation. It is however common to see a paragenesis suggesting that folding is earlier than the brecciation. (b) and (c) are other examples more typical at various scales of "broken" recumbent folds with sub-horizontal axial planes floating in a carbonate breccia matrix (scale bar in (c) 5 m). Folds are also truncated by sub-horizontal depositional scars (d). In (d) also note the complexity of some folds that can be non cylindrical and be refolded during progressive strain (scale bar 2 m).

A second diagnostic feature of the Century cover is the occurrence of depositional or erosional scars that truncate slumps (e.g. Smith, 2000). The synsedimentary truncation appears to post-date the folding event (Fig. 6.6a) suggesting a syn-depositional age for the folds.

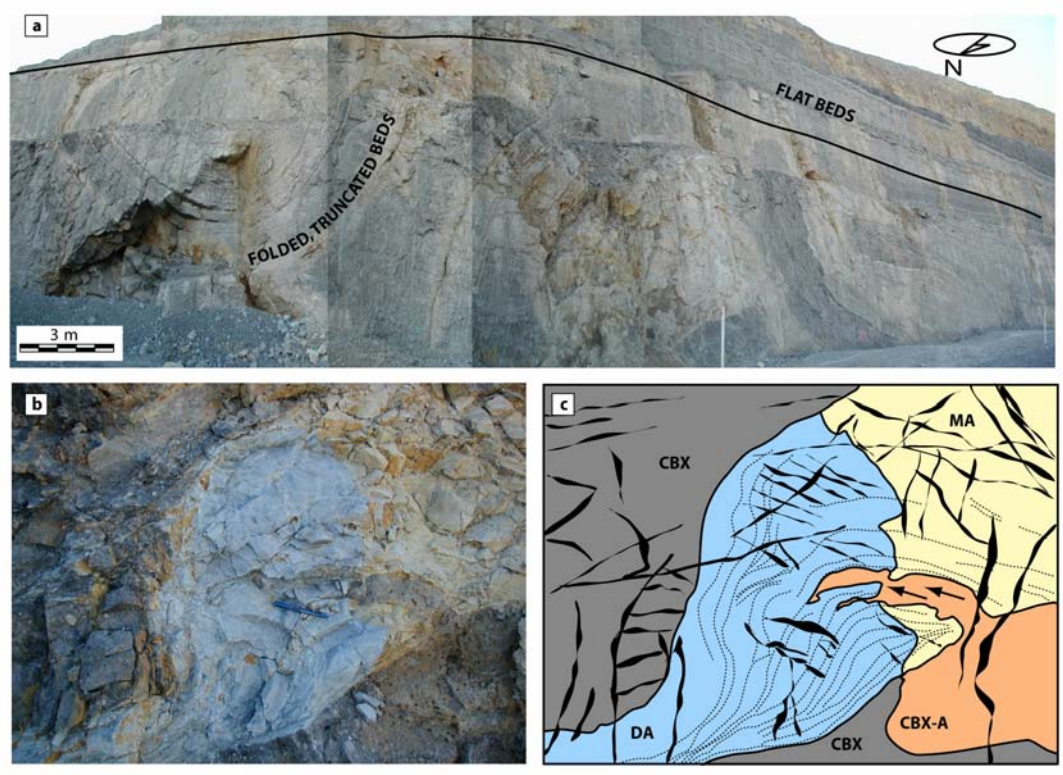

Fig. 6.6 Cross section view of a depositional scar (black line) truncating highly deformed layers of dolomitic grainstone superposed by flat laying undeformed strata. Folds of variable amplitude and interlimb angle abut laterally against broken beds. Often depositional scars are filled with discontinuous pods of marl (b, c) that are locally fractured and folded as shown in the previous figure and in enlarged view here (cf. Fig. 5a with 6b, c). Notice also that a later phase of alteration overprints marl and carbonate breccia injections. Fracturing and jointing postdating hydroplastic deformation represents the latest style of deformation.

6.4.1.3 Slump development

van Loon (2003) remarks that it is possible to reconstruct the original position of a palaeoslope by considering the orientation of overturned strata in sedimentary slumps; however, tectonic overprinting causes anomalous geometrical patterns (Potter and Pettijohn, 1963; Elliott and Williams, 1988). Slumps form in response to palaeoslope instability induced either by gravitational or coseismic activity. The strain distribution is variable along a slump front and commonly produces a curved fold axis. Variation of structural morphology and orientation of folds can be also due to sedimentary influences such as switching of palaeocurrent directions on the palaeoslope, and also flow induced rotation of fold hinges (Allen, 1982; Smith, 2000). It has been demonstrated that in some circumstances slump folds might have a consistent orientation (Kuenen, 1967), but in several other cases (including the study presented here, see Fig. 6.7a-e) they may vary. Following Smith (2000), slump sheets or lobes can be considered to include a central zone C, and a flank zone F (see, Fig. 6.7a). The fold axis is commonly orthogonal to the direction of flow, although along the flanks (F), it may display different orientations compared to the centre (C). This may result from rotational dragging or divergent flow of the slump (Smith, 2000).

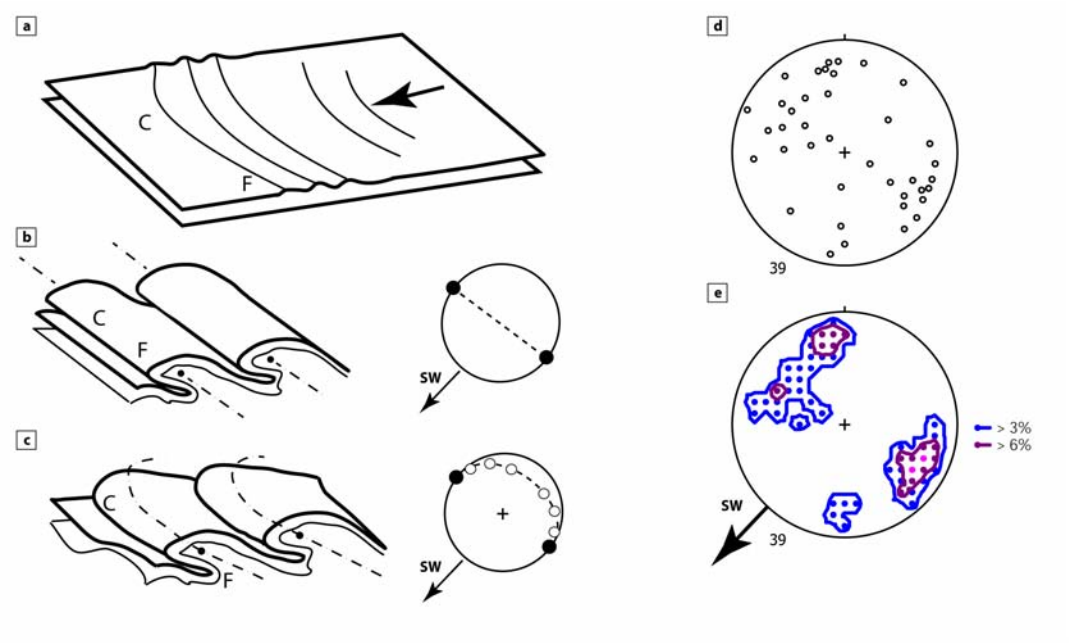

Fig. 6.7 Conceptual models of slump fold development induced by sliding along bedding planes (a, b, c). Comparison of (b) with (c) suggests that one of the causes of misorientation of fold axes is intrinsic to the mechanism of fold development that involves rotational dragging of the flanks (F) in respect to the central front of slump propagation (C). The data collected in the mine area and projected here in (d) as poles of planes in a lower hemisphere projection and in (e) as percent distributions could be interpreted as resembling a girdle distribution considered in (c). However, several other components have conditioned the final orientation of measured structures.

The stereographic projection in Fig. 6.7d displays the orientation of thirty nine fold axes collected along the eastern, northern, and western walls (stages 3, 4, 5) of the Century Mine. Measured fold axes could be interpreted as randomly oriented and this might be partly caused by tectonic titling of strata during faulting and rearrangement of large blocks entrained in the fluidised breccia matrix (e.g. Fig. 6.4a). However, the plot of the density of distribution of fold axes shown in Fig. 6.7e, suggests, alternatively, that recumbent folds might be slumps linked to an extensional stress-field with $\sigma 3$

approximately northeast-southwest striking. Slumps may have been developing along a basin slope dipping southwest, an orientation compatible with the location of the closest topographic high in the area (Gum Hole Plain) (see Fig. 6.1c).

6.4.2 Lawn Hill Megabreccia

The most prominent structural character of the Thorntonia Limestones, beside the large recumbent folds, is the widespread occurrence of breccias. The extensive brecciation observed in the Century open cut represents an assemblage of various lithotypes described in Szulc (1992) (Fig. 6.8a, b). Here the different types of breccia composing the Lawn Hill Megabreccia (this term is used to group all types of breccia observed in the study area) are described. Their temporal relationships and spatial distribution is also discussed.

Analysis of spatial associations between faulting and intrusions (CBX) is another important feature of the Lawn Hill Megabreccia. This character can be used to evaluate the importance of faulting in the process of redistribution of cover material during basin evolution. It may be difficult to quantify the spatial distribution of carbonate dykes where they cut similar lithologies (e.g. dolomite dykes in dolomitic limestone). However, in the Century area the carbonate dykes/sills penetrate the underlying, siliciclastic basement. This makes the assessment of their distribution and orientation relatively easy. Dyke geometry is used to evaluate the possible palaeostress

direction when the dykes were intruded. This is then compared with other structural indications of the likely palaeostress directions.

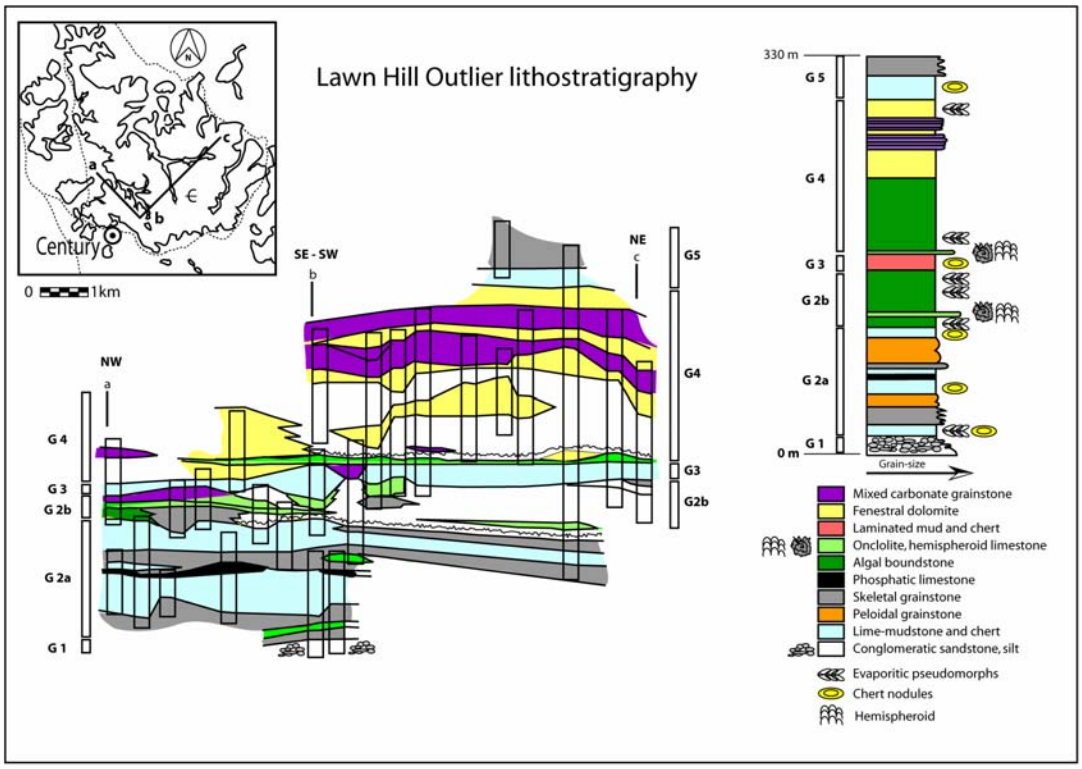

Fig. 6.8 Lithostratigraphic classification, redrawn from Szulc (1992). The stratigraphic section through the annulus offers a perspective of the spatial variation of lithofacies. Notice the shift from deep ramp facies to more inter/supratidal settings inward. The summary of lithostratigraphic variation outlines several marker beds containing allochems such as onkolites and shell-beds (coquina like, e.g. see Loi and Dabard, 2002), often represented by cherty concretions. Also hemispheroids are reported by Szulc (1992).

6.4.2.1 Varieties of breccia

The Lawn Hill Megabreccia displays a various petrographic nature. Several processes contributed to its formation, but also transformed the breccia during basin evolution (e.g. alteration, later deformation etc.). Here we propose a subdivision of the breccia depending upon their textural variety. The term Lawn Hill Megabreccia encompasses all the distinguished end-members, because the megabreccia is considered the final assemblage of multiple phases of breccia developed at different times and from different mechanisms. The distinctions made are then used to infer a possible origin for the different breccias. Notice that diverse breccias may have been coeval, but forming from different genetic processes (e.g. a debris-flow breccia can be formed in a slope setting; whereas contemporaneous sub aerial exposure of shelfal limestones may cause karst-breccia development). Alternatively, multiple types of breccia could be forming also as function of their different time of formation during basin evolution (e.g. debris-flows can be deposited on the seafloor then reworked and redeposited by marine currents, or injected in fractures and faults at later time during diagenesis). Analysis of cross-cutting relationships provides a way to reconstruct a temporal evolution for the different breccias allowing a better understanding of these processes.

The Lawn Hill Megabreccia is more than 200 m thick on the northern side of the Century Mine (stage 4, Fig. 6.4a) and consists of a carbonatic to dolomitic groundmass with huge floating clasts up to hundreds of metres across (Fig. 6.4a, b). The nature of the clasts ranges from monomictic to polymictic. The breccia is composed of

carbonates, marls and cherts with a variable degree of sorting, and also variable rounding of the clasts. The matrix/cement composition varies in a similar manner according to the clast composition, and can be abundant, forming matrix or cement-supported aggregates, to scarce or lacking in clast-supported aggregates.

The geometrical relationship between breccias and host is variable providing additional information on their likely origin. Breccias are distributed both in the Middle Cambrian limestone, and also as sills and dykes in the Mesoproterozoic siliciclastic basement.

In the cover the spatial association of breccia to host is diverse, with the breccia occurring either as dykes (Fig. 6.9a) or sills, but also occurring in limestone cavities, distinct by their irregular outline and by evidence of collapse related fragments detached from their roof (Fig. 6.10a-c). The carbonate breccias also occur as stratiform bodies that extend for several 100's metres. Locally these beds preserve grading and sorted clasts. In the basement, breccia dykes and sills are exclusive - there is no evidence of collapse/solution related cavities or bedded tabular breccias. Sub-vertical dykes are (1 to 30 m) commonly thicker than shallow dipping sills (1 to 5 m), and often sills terminate a few metres away from the connected dykes suggesting, mostly, vertical transport of breccia material (Fig. 6.9b). The biggest example of dyke penetrating the basement is located on the northwestern corner of the pit (stage 4, Century Mine, see Fig 6.4a). The sub-vertical dyke is approximately 30 m wide, its termination into the basement is complex with sills departing laterally and causing jacking of bedding planes in the basal, Mesoproterozoic shales.

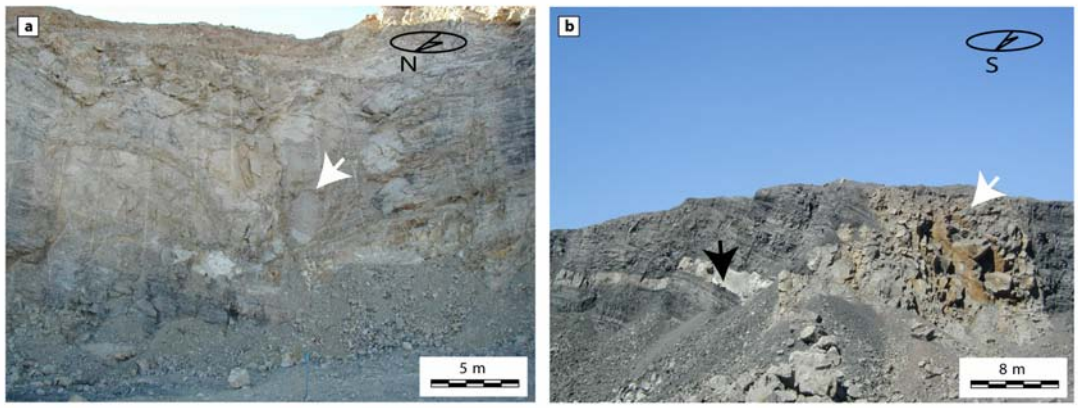

Fig. 6.9 Examples of steep dipping intrusions in Middle Cambrian cover (a) and Mesoproterozoic basement (b) (arrows for dyke/sill location). In (b) the thickness distinction made in the text is outlined. Dykes are generally thicker than sills (black arrow) when penetrating the basement (see also Fig. 4a - GD).

Based on the considerations made, and on textural features described below, we propose a subdivision following the Universal Rudrock Code (Laznicka, 1989; Jebrak, 1997). Four types of breccia were distinct (Fig. 6.11a-f):

1. Flow Breccia (CBX).
2. Flow Breccia (MB).
3. Solution Breccia (SB).
4. Collapse Breccia (CB).

Note however that the some breccias grade into one another (see below).

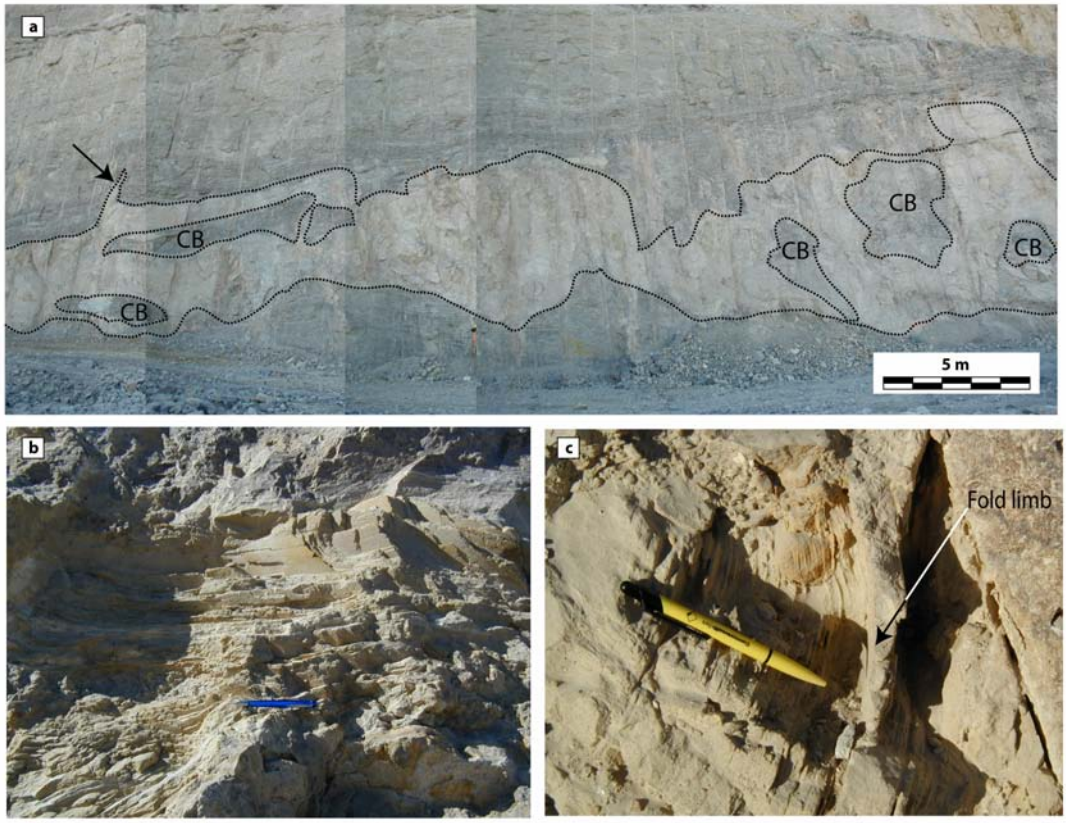

Fig. 6.10 Examples of interpreted solution/collapse cavities in cherty limestone exposed on the western side of the Century Mine (Stage 5). (a) Solution cavity filled by CBX breccia. The breccia has also infiltrated the roof of the cavity that formed in relatively undeformed limestone (see arrow). Note collapsed bedded intervals now floating in the carbonate breccia matrix (CB). Some cavities host bedded sediments such as calcarenites (b and c), beds are flat lying within cavities but may also develop slump folds (c) (pen for scale).

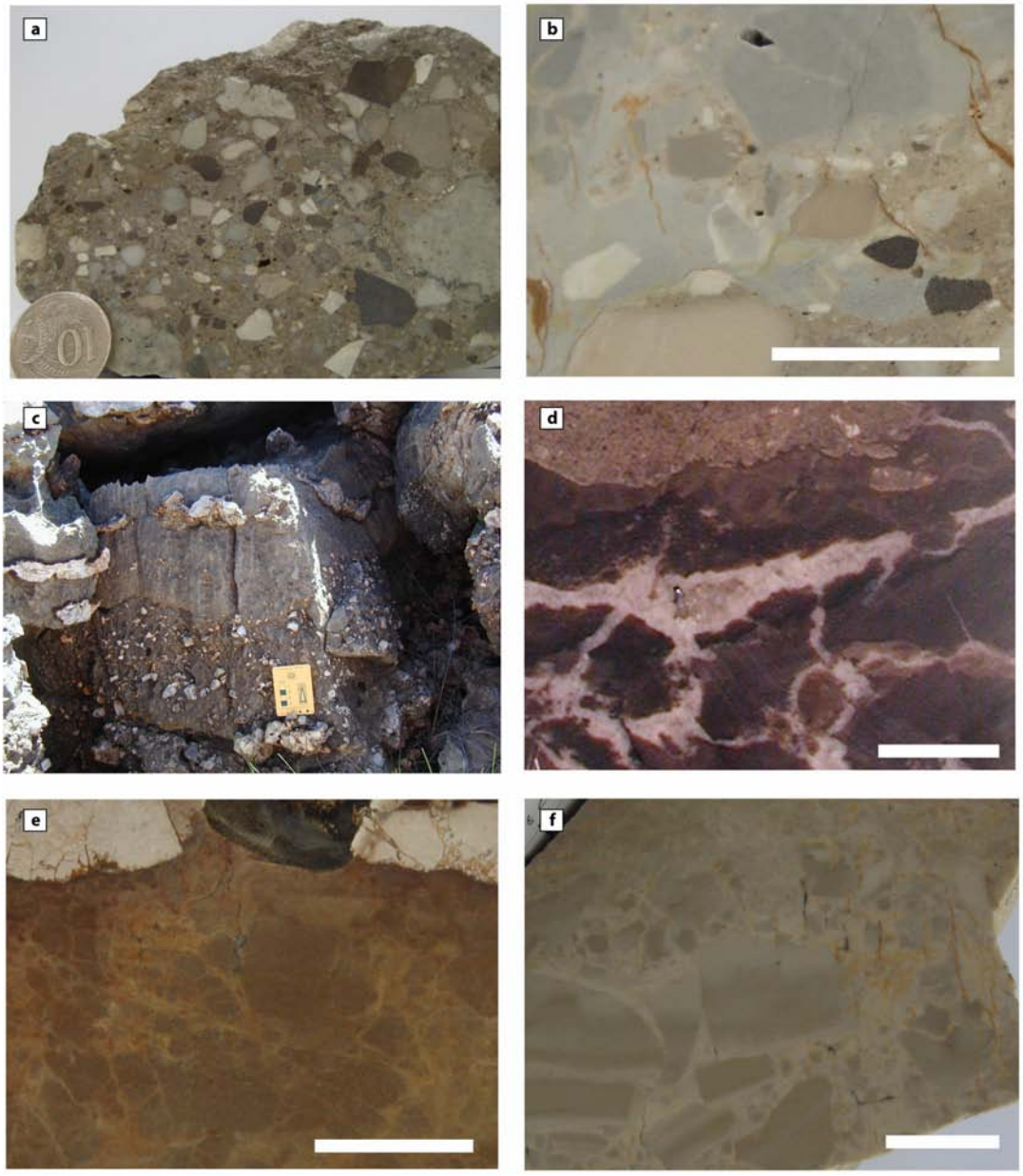

Fig. 6.11 Breccia typologies observed along mine exposures, and also in drill core and outcrop, in the more internal part of the annulus. (a) Polymictic, CBX breccia, the most common variety in the Century mine forming sills and dykes that penetrate cover and basement. (b) Mixing between flow breccia (MB) and a CBX sill (scale bar 0.5 cm). The two end-members mix together gradually and produce an admixture of broken clasts and groundmass representing a composite breccia. This evidence is suggestive of a similar state of consolidation of marl and CBX indicating penecontemporaneous deformation. (c) Stratiform, solution breccia, composed predominantly of chert angular fragments likely derived from siliceous concretions. Grainstone/packstone (d, e) and also oolitic, dolomitic sandstone display corroded

clasts aggregated by calcitic or dolomitic cement(scale bars (d) 1.5 cm and (f) 0.5 cm). (f) Collapse breccia in crystalline dolomitic limestone (scale bar 1 cm). Normal grading and rounding may indicate local transport although the monomictic nature of the clasts is more indicative of local sourcing from adjacent proximal limestones. Local reworking may be explained also with tidal currents that would allow rounding although with limited transport of the clasts that tend to be trapped on the bottom of the cavity (Appendix D for specimens spatial location).

6.4.2.2 Flow breccia CBX

The Flow Breccia (CBX) is the most common variety of breccia across the whole outlier and the only one occurring both in cover and basement (Fig. 6.9a, b). The breccia occurs as dykes and sills and also as infill in irregular cavities (Fig. 6.10a-c). CBX dykes and sills have variable width from a few centimetres to 10's of metres. Sills do not cross-cut dykes and they both have same infill material. CBX dykes locally cross-cut Flow breccia (MB) dykes (another variety of breccia). However, in some cases the two breccias grade into one another and mix together. The clasts include both folded and unfolded fragments derived from the Middle-Cambrian cover, but also from the Proterozoic basement - one of the largest blocks was originally part of the Century orebody (Eastern Block, Fig. 6.4b). Frequently, at larger scale (100's of m) the breccia becomes chaotic with domains filled by groundmass separated by other domains characterised by clast-supported megablocks of carbonate strata. The size of the clasts (excluding the megablocks) is variable from millimetres to metres (typically between 0.5 and 60 cm) (Fig. 6.11a). When the breccia occurs in dykes and sills the clast size is function of the conduit size that causes sorting; therefore, the breccia could be

considered as a coarse, sub-rounded to angular fragmentite that becomes a microfragmentite when infilling narrow fractures and faults. The CBX is polymictic including three varieties of clasts recognised in hand specimen and thin section: (1) lithic clasts of carbonate; (2) cherts and (3) fragments of Mesoproterozoic basement, siltstone/shale. The groundmass composition corresponds to the fragment composition with matrix more abundant than cement. The sandstone/siltstone carbonate matrix supports the clasts of the CBX breccia and is petrographically analoguous to dolomitic limestones occurring predominantly in the upper part of the lithostratigraphic subdivision group G4 of Szulc (1992). The cement is composed of a mixture of calcite, dolomite, quartz, and iron oxides. This type of breccia can be considered transported because of the occurrence of rounded clasts and also because of its polymictic nature. Its occurrence in the basement represents an additional indication of movement exceeding 10's of metres. The close analogy between the CBX matrix and the sandy dolomites of the Thorntonia Limestone, and Border Waterhole Formation may suggest a derivation from these lithofacies. Alternatively, unconsolidated sandstones may have been deposited as debris-flows and turbidites in the present sites before lithification. Local evidence of clast segregation and normal grading may favour this interpretation (see, Fig. 6.12a, b). The breccia appears to have been emplaced in a temporally confined event before matrix consolidation, because apparently there is no evidence of recemented fragments of matrix in CBX, a feature that should be evident if brecciation and emplacement of CBX occurred during a protracted timeframe of basin evolution, involving reactivation and multiple injection events.

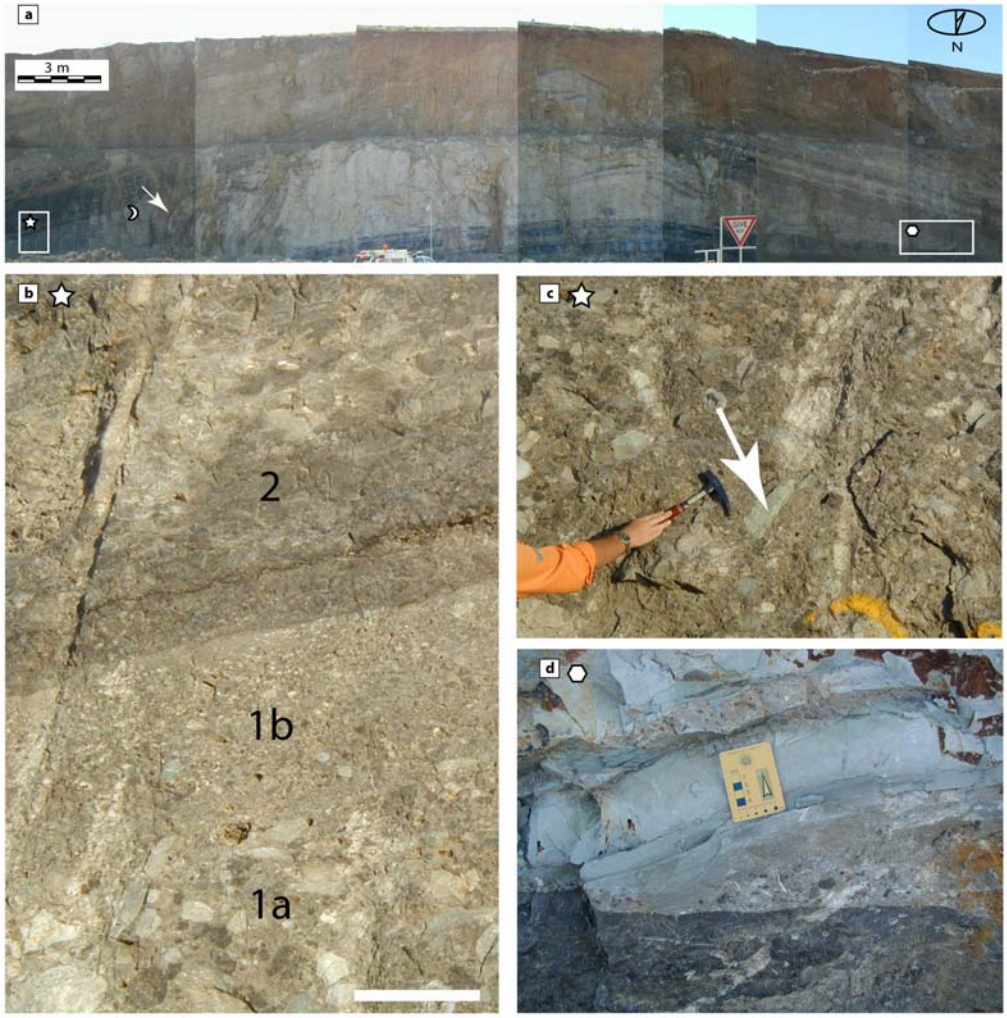

Fig. 6.12 Slumping initiation in relatively undeformed beds of the Thorntonia limestones. (a) Landscape view of a tepee like structure, carbonaceous siltstones and marlstones, distinguished for their dark (carbonaceous colour) and fine grained lamination bound the top and basal part of an intrastratal mass-flow to debris-flow body that has suffered internal reorganisation during slumping. The CBX breccia locally preserves graded beds that formed probably along the slope during debris-flow deposition. (b) Illustrates an example of debris-flow deposit with size segregation of clasts (scale bar 30 cm). A basal unit (1a), of clast supported carbonates, cherts and basement fragments (c) is overlain by matrix-supported and well sorted clasts (1b) of similar provenance. The bimodal admixture is sealed by mud supported carbonate chips (2). As a debris-flow moved basinwards, its sediment concentration and strength progressively decreased due to the entrainment of the ambient seawater. Probably the reduced shear strength and decreased flow viscosity allowed vertical segregation of clasts, resulting in a two-storey debris-flow (e.g. Payros, 1999) (star symbol for sample location, cf. with (a)). (d) On its eastern side (hexagon symbol site) the sedimentary breccia loses its patterning becoming a chaotic assemblage of carbonate sediment indistinct from CBX and partly mixed with coalescent marl.

6.4.2.3 Flow breccia MB

The Flow breccia (MB) was recognised only in two locations within the Century Mine. Its occurrence is limited and stratigraphically constrained to intervals proximal to thin laminated strata of marl (grey-blue in colour). Their occurrence was observed either in the basal part of the megabreccia proximal to the interface with the basement, but also in upper stratigraphic intervals of the Thorntonia Limestone, interbedded with phosphatic limestone and algal boundstones (G2b – G4). Locally the marl beds also form lenticular bodies (Fig. 6.10a). The marls never exceed 5 m thickness and locally, where deformation is more intense, they represent a source for flow breccia dykes that intrude cherty and phosphatic limestones (Figs. 6.6b, c and 6.12c). MB dykes are frequently cross-cut by CBX (Fig. 6.6b, c) or grade into CBX (Fig. 6.12c). MB fragments rarely exceed boulder size (25 cm). The breccia could be defined as angular mesofragmentite. It is also distinct from the CBX for its monomictic nature although it becomes polymictic when mixed with CBX (Figs. 6.11b, 6.12c). The matrix corresponds to the fragments composition, but locally the cement is more abundant and calcite-rich. The fabric is fragment-supported with interfragmental space filled by variable groundmass. This breccia is interpreted as transported, although the distance of transport is considerably less (within 10's metres) than the transport suffered by the CBX. The MB dykes appear to have been emplaced when the marl was partly lithified as they display hydroplastic deformation (e.g. slumps). The gradual mixing of CBX with MB is also indicative of a non lithified condition of both breccias. The rock micro-

fabric indicates a possible mixed component of intergranular movement and cataclastic flow. This may be due to a partial consolidation of the marls or alternatively by multiple phases of deformation. In thin section the MB dykes contain quartz micro-clasts displaying variable undulose extinction, but also apparently preserve undeformed crystals of quartz (homogeneous extinction across the area of the crystal). This textural feature may be the result of a semi-brittle state of the marls during deformation (see Maltman, 1984).

6.4.2.4 Solution breccia

The Solution Breccia (SB) is exclusive to and intrastratal within the Cambrian limestones (Fig. 6.11c) and occurs in horizons frequently associated with halite and gypsum pseudomorphs (see Henderson and Southgate, 1980; Szulc, 1992, groups G2a, G2b and G4). There is no clear cross-cutting relationship among SB and CBX or other breccias. The size of the clasts is variable with a range between 0.5 and 15 cm. The breccia can be classified as an angular mesofragmentite with a single fragment variety composed of chert. The groundmass composition semi-correspond to the fragment composition. The matrix is composed of calcarenitic, lobated micro-clasts, which are floating in dolomitic/calcitic cement. SB is matrix supported and likely formed from solution of its host. This is suggested by the corroded aspect of matrix clasts. Angular monomictic clasts indicate a minimal transport. Notice that the matrix is analogous to the oolitic, dolomitic sandstones of the Thorntonia limestone and Border Waterhole

Formations. The corroded nature of carbonates micro-clasts (Fig. 6.11d, e) is indicative of pressure solution involving mainly calcite and possibly halite and gypsum. Solution breccias may have been precursors of CBX breccias. The two breccias share similar matrix composition, and progressive transport may have been controlling mixing with other carbonatic components, causing selective rounding of clasts and transforming SB into CBX type breccias.

6.4.2.5 Collapse breccia

This type of breccia was recognised in a block of dolomitic limestone (200 m width) occurring at the base of the Lawn Hill Megabreccia, on the eastern side of the Century Mine. The CB has limited extent and is found exclusively in compact thick bedded limestone. Locally CB is crosscut by CBX (which postdates it), and also is found as infill of irregular cavities in limestone. Clasts have variable size ranging from 0.2 to 6.4 cm. The breccia is an angular to sub-rounded mesofragmentite and is monomictic with clasts composed of limestone. The cement is micritic limestone, corresponding to the clast composition. The amount of interfragmental filling is variable, with a fabric variation from clast supported to predominately matrix supported in the top part of the sample (Fig. 6.11f). This textural variation suggests possible gravity or local flow induced sorting during rock fall. CB likely underwent minimal transport (on the order of metres) considering its monomictic nature and the close association to its protolith. A possible explanation of the origin of this breccia would be a collapse of limestones due

to the formation of karstic cavities. Karstic cavities have been identified in the pit and elsewhere in the Lawn Hill Outlier. Alternatively, the fragmentation might be associated with fault movements.

6.4.2.6 Overprinting relationships

CBX, MB, CB, as seen, have distinct temporal relationships among them that can also be useful to further constrain the timing of recumbent folding. A paragenetic chart is proposed in Fig. 6.13. The sequence of cross-cutting relationships could be interpreted as follows: (1) after limestone/marl sedimentation, slope instability caused debris-flow and turbidites leading to the deposition of sorted and segregated clasts forming graded CBX breccia. Further destabilisation of the limestone caused also the development of slumps and redistribution of unconsolidated CBX, followed then by hydroplastic redistribution in dykes and sills of thin marly intervals. The evidence of folded marls (Fig. 6.6b, c) suggests that their hydroplastic deformation and recumbent folding were synchronous at start. Folded marls are cross-cut by CBX breccia that is unfolded. CBX also entrains blocks of limestone containing recumbent folds suggesting that it may be postdating the slumps. However, the gradual mixing observed between CBX and MB supports the alternative interpretation that hydroplastic redistribution of marls and CBX intrusions were synchronous. Therefore, a synchronous emplacement of CBX during penecontemporaneous slump folding cannot be excluded. Finally if the CBX event was relatively early, then also CB formed early because limestone cavities

are filled by CBX. The temporal collocation of SB remains uncertain but likely it shares a common timing with the CB breccia, because cavities initially tend to develop by dissolution followed then by a collapse and CB accumulation in limestones.

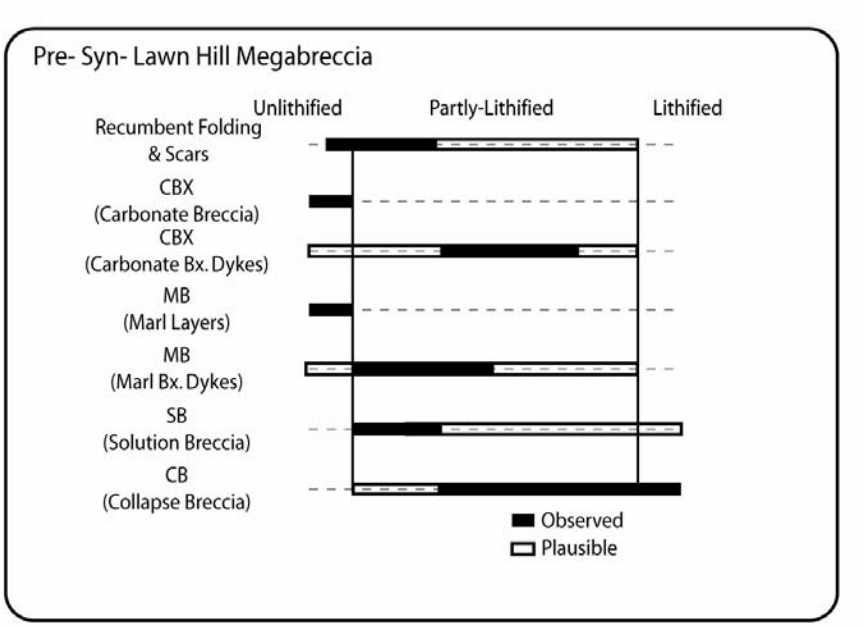

Fig. 6.13 Paragenetic chart illustrating the initial phases of basin evolution involving slump/scar development, the formation of different breccia types, and their evolution (see text for discussion).

Fig. 6.12a shows an interpreted tepee structure with a series of examples of CBX and MB breccias interrelationships. Tepees are expansion polygons with deformed raised edges formed by a volume increase of the associated sediments, accomplished by in situ, near surface, displacive growth of evaporites or carbonates (Gandin et al., 2005). Tepees may be also produced by gravitational collapse and

redistribution of partly lithified sediments, because their injection causes local increases in volume. The whole structure appears as an internal, stratiform body of CBX delimited on top and bottom by massive and deformed limestones. Locally the limestones are folded (e.g. the limbs of a recumbent fold are outlined in proximity of the core of the tepee structure, Fig. 6.12a, see arrow) and also they resemble imbricated stacks. Fig. 6.12b-d illustrates various styles of CBX breccias. Observed textural and structural appearances are in the first case (Fig. 6.12b) suggestive of a sedimentary deposition in a debris-flow deposit (this would be also an indication of slope instability) that evolved in a turbiditic current. In contrast, the chaotic mixing of marl and carbonate breccia (Figs. 6.12c, 6.6a, b) is interpreted as a sign of later injection of MB breccias.

The temporal relationships among CB and CBX are illustrated in Fig. 6.10a which outlines the infill of a limestone's cavity by CBX. Occurrence of bedded and slumped sandstones has been also found in other cavities (Fig. 6.10b, c). These evidences coupled with the textural evidence provided in Fig. 6.11e are suggestive of karstic collapse. Dissolution has contributed to the development of cavities in more massive carbonate strata that were subsequently filled by a groundmass of variable composition (CBX, MB, CB, SB).

A synergy of described genetic processes may have been contributing to the Lawn Hill Megabreccia development. However, considering the relative abundance and distribution of CBX breccia and the scale of slump folding, it is easier to invoke the transport component (1) as the dominant process at least for the Century area.

6.4.3 The control of basement faulting and fracturing on the CBX megabreccia distribution

Statistical correlation analysis was allowed by the available 3D reconstruction of the Century Zinc deposit (Feltrin et al., 2006), which represents a 3D virtual environment where spatial analysis can be undertaken to allow better geological interpretations. The analysis is focused on CBX-type breccia, The most widespread in the Century Mine, but also confined to dykes and sills occurring in basement.

6.4.3.1 Importance of spatial analysis in establishing the palaeostress direction

A structural analysis of the orientation of dykes in basement is proposed as a useful way to infer the direction of the palaeostress field during their emplacement. Palaeostress directions can be compared with the inferred spatial orientation of the palaeoslope, to ascertain if dykes were emplaced in a stress field that would have been favoring the slumping observed. Similarly, the palaeostress direction may be compared with other potentially younger tectonic structures to check on possibilities of reactivation or syntectonic brecciation.

Fractures that host injected materials may have been tensile, in which case they propagated orthogonally to the least compressive stress direction (Delaney et al., 1986; Boehm and Moore, 2002). This may be recognized by swarms of commonly oriented dykes. However, dyke patterns can be controlled by pre-existing structures prone to reactivation during subsequent deformation (Pollard, 1973; Jolly and Sanderson, 1995; Boehm and Moore, 2002), and they may also have intruded at angles oblique to $\sigma 3$ if they were acting as normal faults, i.e. shear failure (Jaeger, 1969 ; Hobbs et al., 1976) (Fig. 6.14a-d).

A 3D structural model representing the Century Mine has been constructed using the software GoCAD (see Fig. 6.15a-e) to obtain a detailed visualisation of breccias and faults in three-dimensional space. Additionally a Visual Basic algorithm was compiled to statistically estimate the trend of carbonate dykes considering their proximity to faults.

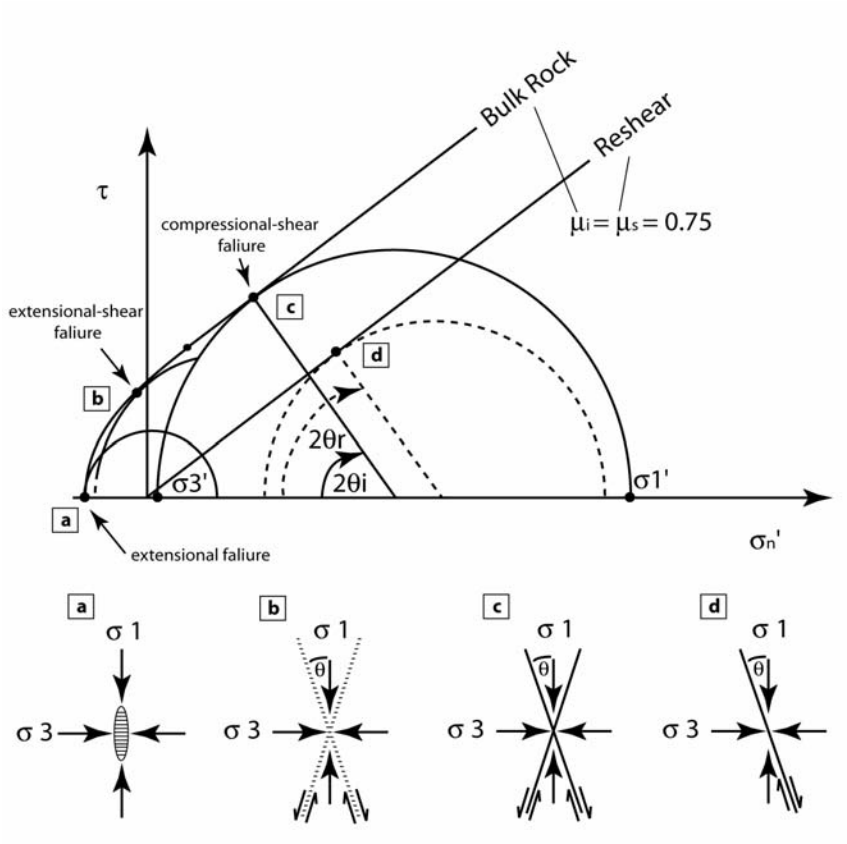

Fig. 6.14 Mohr diagram of shear stress, τ, against effective normal stress, σ_n' with a composite Griffith-Coulomb failure envelope for intact rock normalised to tensile strength, T, illustrating the stress conditions for the three different modes of macroscopic brittle failure, plus the reshear condition for an existing cohesionless fault (the internal friction μ_i is assumed for simplicity to be equal to the sliding friction angle and both are averages of experimental determined values) (adapted from Sibson, 2000). The four criteria of brittle failure are also presented with their relative orientation with respect to the stress field assuming a projection plane orthogonal to σ_2: (a) extensional; (b) extensional-shear; (c) compressional-shear and (d) reshear of cohesionless fault.

Comparative visualisation of the spatial distribution of CBX and faults outlines a close correlation between the spatial location of faults and the spatial location of CBX dykes. In addition the orientation and distribution of CBX in several examples matches the fault patterns (see Fig. 6.15e). Therefore, proximity to faults has been used as a likelihood parameter to infer the spatial orientation of CBX breccia dykes and sills. Fig. 6.16 illustrates the various fault orientations that more likely host CBX dikes in the Century Mine. Shallow dipping structures (Fig. 6.15a), and steep dipping faults are present both in cover and basement. The predominant trends of steep dipping structures are NW-SE (Fig. 6.15d, e), an orientation consistent with one of the major Mesoproterozoic faults in the region (Termite Range Fault) (Feltrin et al., 2006). Also prominent are NE to NNE trending faults (Fig. 6.15c), characterised by multiple sets of slickenlines recording multiple directions of movement (either dip-slip or strike-slip). E-W faults are also documented (Fig. 6.15b) and represent a system of lateral splays of the Termite Range Fault forming a half-graben, which hosts the Century deposit. These structures display a large dip-slip component of movement (e.g. Pandora's Fault) that can exceed hundreds of metres. There is consistency between orientations of faults that were mapped in the cover with documented orientations of corresponding structures measured on mine benches in basement, suggesting possible reactivation of basement faults.

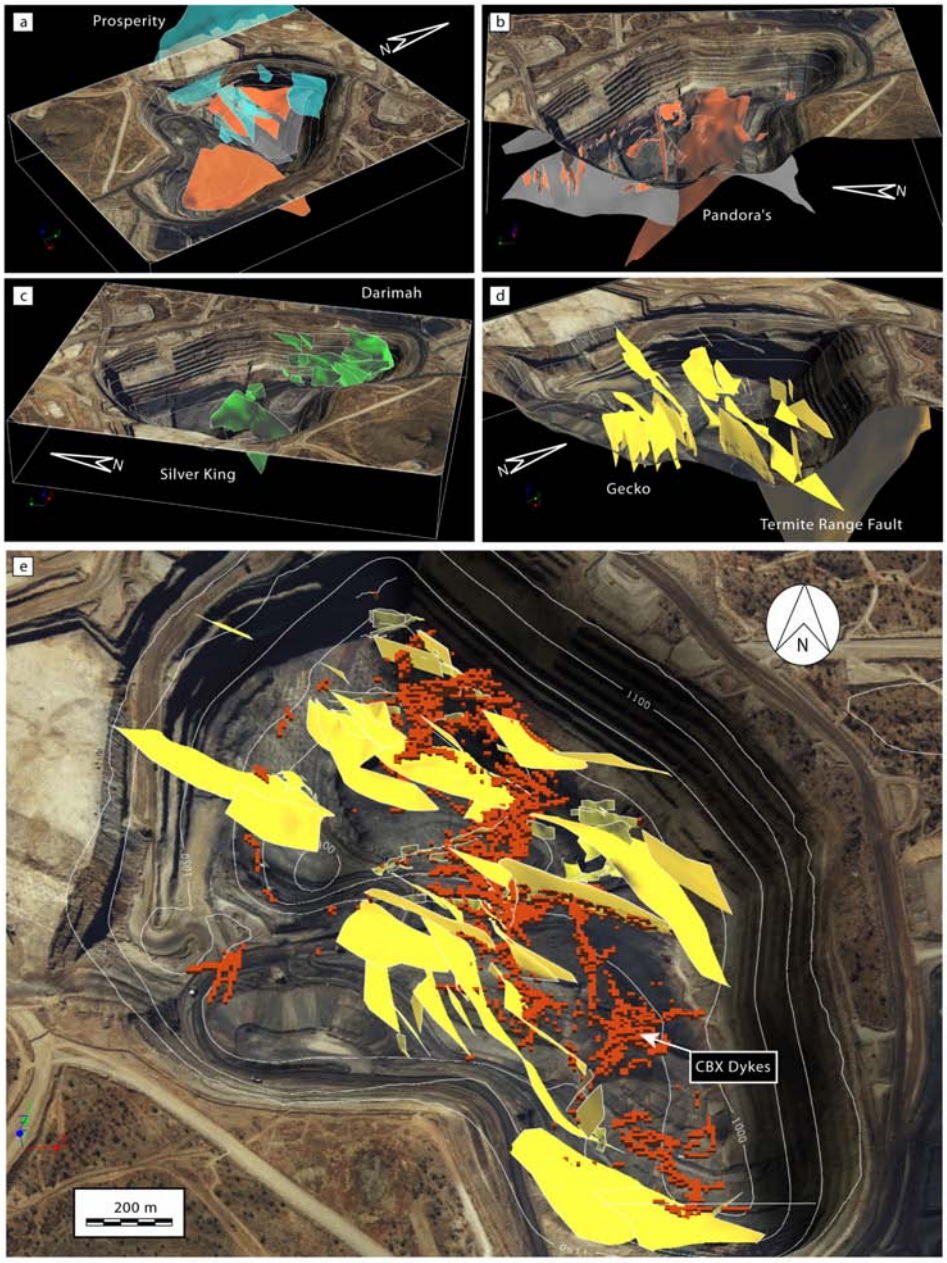

Fig. 6.15 3D structural/CBX breccia model of the Century Mine. (a), (b), (c) and (d) illustrate the modelled fault systems intersecting cover and basement with relative (fault systems are referred into the text using the mine terminology). (e) represents a top view of the pit showing the Gecko System and other faults with similar orientation that in places display a strong association with modelled spatial distribution of dykes (CBX) (hosting the Century Zn-Pb-Ag mineral deposit). Breccia dikes follow mostly WNW trends but also N-S, NE and NW trends are common.

6.4.3.2 Quantitative estimation of the spatial distribution of dykes

The abundance of dykes in the basement decreases from east to west across the mine area. This is a function of the spatial location and continuity of faulting and fracturing throughout the mineral deposit. Frequently, the dykes become more prominent and abundant at fault intersections (Fig. 6.15e). To better describe the variation in concentration and orientation of dykes, sub-sampled distributions of CBX were integrated in a voxet model (Fig. 6.15e). Two main datasets were considered, to statistically estimate the spatial orientation of CBX dykes: (1) fault distributions and orientations reduced to pointset data (X, Y, Z, Dip, Azimuth); and (2) the spatial distribution of dykes (X, Y, Z) occurring in drill core and exposed in the pit. A software program was then used to compute Euclidean distances between these two datasets (see Appendix C), using the following equation:

$$d = \sqrt{(x_i - x)^2 + (y_i - y)^2 + (z_i - z)^2} \quad (6.1)$$

Calculated distances (*d*) were used to find the closest orientation (x, y, z) of a fault to a generic voxel (xi, yi, zi) containing CBX breccia. This provided the most likely orientation of a dyke based on fault data at a maximum of five metres interval (d). Plots for different (d) are presented in Fig. 6.16. The results were also classified depending on the dip of the dykes. Dykes with less than 30 degrees dip were classified as sills, while dykes with a dip angle (D) between 30 and 60 degrees were defined as

oblique. Finally, sub-vertical dykes dip between 60 and 90 degrees. The equal area projections show multiple and either persistent or variable patterns, as a function of interpolation distances. For example the sills appear to be focused in two clusters within all the four plots (<2-5m), suggesting that dips vary gently between 0 and 30 degrees. In contrast, the focussing of normal poles in the first and third quadrant (clockwise notation) is indicative of discrete planes striking from north-south to northwest-southeast. Oblique dykes have poles prominently distributed in the second and third quadrant and small isolated clusters of poles suggesting a minimum of four subsets of faults/dykes orientations. NW- and NE-striking systems are prominent. Sub-vertical dykes have persistent patterns, although extending the interpolation distance causes an increasing spread of the point distribution. However, a noticeable pattern with fairly concentrated point distributions is evidenced in the <2m plots. This suggests that most of the steep dipping dykes have WNW strike and can either dip toward NNE or SSW apparently forming a conjugate dip-slip system. Finally a system of faults/dykes that strikes NNE and dips toward WNW is also prominent.

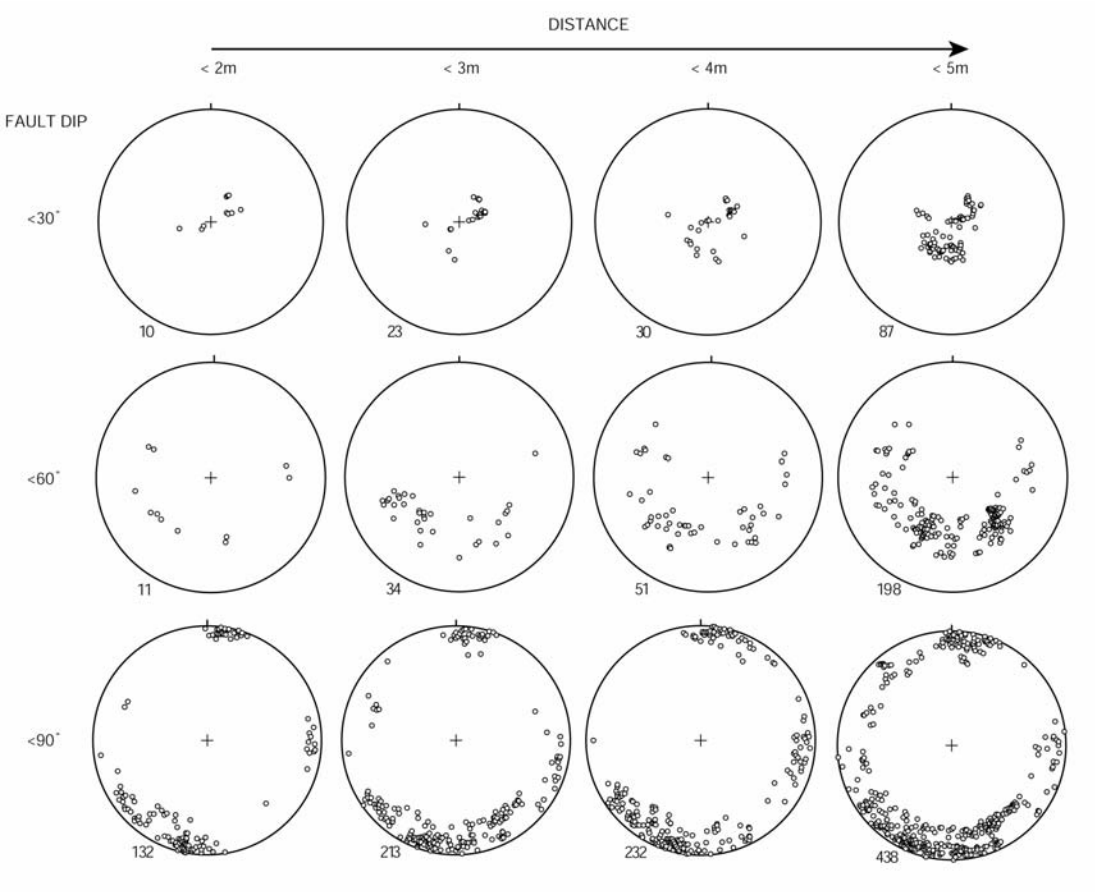

Fig. 6.16 Stereoplots of fault planes proximal to voxels containing CBX breccia, see text for discussion. The distance parameter is the neighbourhood space between spatial location of carbonate breccia and faulting. The number of intersections between CBX breccia and the modelled fault network increases for larger distances although this leads to higher background and consequent girdle distributions. Numbers on the bottom left are the sample totals

In summary the statistical model suggests that more likely the dykes formed mainly within NW and WNW striking structures, and to a lesser extent along NE and NNE directions. This may indicate that all major fault systems of Proterozoic age experienced at least local extension or reactivation to allow the intrusion of dykes

during the Middle Cambrian. Most fault systems are interpreted as initiated during Proterozoic time because they share a similar hydrothermal history (Feltrin et al., 2006). Clearly at least some of the preserved geometries may have been exclusive of the Georgina Basin extensional history.

To further understand the palaeostress history during dyke intrusion, three contour plots for the classes D<30; 30<D<60; 60<D<90 are shown in Fig. 6.17. Each plot contains poles of planes calculated for distances D < 5 m, and was compared with the respective eigenvectors/eigenvalues (see Table 6.1). Eigenvectors/eigenvalues were determined using the software StereoWin (Allmendinger, 2002), which makes use of the Bingham method of Fisher et al. (1987) to compute the scalars and vectorial components of the orientation matrix. Each population of directional data is generally fitted to the Bingham distribution, to test how closely the population's mean (and its dispersion around the mean) fits the distribution for a chosen confidence interval (e.g. Marcotte and Henry, 2002).

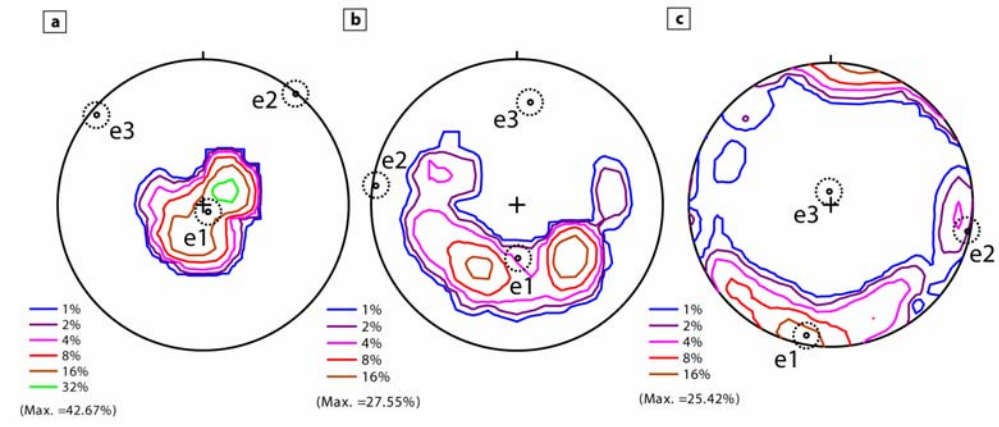

Fig. 6.17 Palaeostress directions (eigenvectors/eigenvalues, e1, e2, e3) for the dip-classes considered in (a) D<30; (b) 30<D<60; (c) D>60 (Fig. 6.16). All plots consider a 5 m correlation interval.

Table 6.1. Bingham axial distributions for sills, oblique dikes, and sub-vertical dikes.

Bingham Axial Distributions								
0° < Planes < 30° dip			30°< Planes < 60° dip			60° < Planes < 90° dip		
Eigenvalues	Eigenvectors		Eigenvalues	Eigenvectors		Eigenvalues	Eigenvectors	
	Trend	Plunge		Trend	Plunge		Trend	Plunge
0.8987	146.5	85.1	0.6558	178.6	55.9	0.7186	190.7	8.2
0.0783	40	1.4	0.2622	274.9	4.3	0.235	100.4	2.4
0.0231	309.9	4.7	0.062	7.7	33.7	0.0464	354.3	81.5

Eigenvalues relate to the basic concept of a deformation matrix (discussed for example in Flinn, 1979). A deformation matrix represents a convenient way to describe the deformation of a rock in three-dimensional space. Three linear equations equivalent to a squared matrix characterised by nine components are sufficient to describe such system. Matrix elements are always real numbers in case of geological deformations. A deformation matrix can always be decomposed to a product of two matrixes, one representing the eigenvalues and another representing the eigenvectors as long as the eigenvector matrix is also square (according to the Eigen theorem Arfken, 1985; Marcus and Minc, 1988). Obtained matrixes provide vectors and scalars that represent the semi-axes on a deformation ellipsoid (eigenvectors) and their relative modulus (eigenvalues) (de Paor, 1983). Considering the relationships between stress and strain, the strain matrix can be thought of as the equivalent of the stress matrix for pure shear conditions. If this is a reasonable assumption, eigenvalues and eigenvectors would reflect respectively magnitude and orientation of orthogonal components of the stress tensor ($\sigma 1, \sigma 2, \sigma 3$) (Flinn, 1979; Boehm and Moore, 2002). Limitations clearly apply in

the case of reactivated systems (Fig. 6.14). Here, statistical analysis provides probability distributions that reflect mixed components derived from multiple palaeostress directions. The plots presented in Fig. 6.17 reflects then the interpreted local variation of $\sigma1,\sigma2,\sigma3$ in space as a function of the orientation of a dyke/sill dilating during injection of carbonate breccia. Notice that calculated eigenvectors/eigenvalues reflect the datasets considered; therefore, they represent a local stress field (voxel based) not necessarily matching a mine-scale palaeostress direction. Nonetheless, measure of the frequency of orientation of dykes (number of voxels containing breccia with a specific orientation) can be used as a weighting parameter in the interpretation of the possible overall trend. Fig. 17c shows the highest amount of data (greatest breccia volume) suggesting that most of the breccia dykes were accommodated by NNE – SSW directed sub-horizontal extension. This consideration is in agreement with evidence of thick sub-vertical dykes at least an order of magnitude larger than sills (Figs. 6.4a and 6.9b).

6.4.4 Post intrusion deformational history

6.4.4.1 Assessing later deformation and fluid flow

To further constrain the timing of emplacement of carbonate dykes, a series of structural features were examined that developed during the syn- to post-burial history

of the Georgina Basin. These features include: (1) sub-horizontal stylolites identified in drill-core (Fig. 6.18a); (2) low-angle to high-angle faults and fractures and sub-vertical joints (Fig. 6.18b, c); and (3) veins (Fig. 6.18d). These structural features are demonstrated to postdate the Lawn Hill Megabreccia event. Carbon and oxygen isotopic analyses on whole rock samples and carbonate veins were also used to understand the possible involvement of fluids during a later tectonic overprint.

6.4.4.2 Timing constraints: stylolites, fractures, joints and veins

A prominent feature observed in carbonate breccia dykes are sub-horizontal macro-stylolites (Fig. 6.18a). Stylolites form during burial and loading in a sedimentary basin typically being oriented approximately orthogonal to $\sigma 1$(Andrews and Railsback, 1997). Dewers and Ortoleva (1990) proposed, on the basis of mathematical modelling and numerical simulations, that stylolites are a product of self-organisation by mechano-chemical feedback. Essentially the host-rock reorganises itself during sedimentary compaction and diagenesis, involving dissolution during stylolitization and simultaneous precipitation elsewhere. Organised networks of fractures and joints may similarly reflect mechanical self-organisation (Zhang and Sanderson, 2002). Reed and Wallace (2004) proposed a minimum depth of formation of macro-stylolites of 800 m. Elevated pore pressure values may inhibit the development of these features even at several kilometres of depth, so timing information derived from these features is approximate. However, because these sub-horizontal stylolites occur in carbonate dykes

(Fig. 6.18a), the dykes must have been emplaced prior to diagenesis at these depths, i.e., Middle to Late Cambrian age at the latest.

Widely distributed and complex fracturing and jointing in the breccia dykes also postdate the emplacement of the breccia. As Price (1966) concluded, it is unlikely that complex fracturing and jointing observed in a geological system could be the result of a single deformational event. In this context, the discrimination of the possible timing of joints and fault reactivation is attempted. Joints can be classified using the approach of Engelder (1985), because they represent particular types of fractures (mode 1, dilational) that typically form orthogonal to $\sigma 3$ (e.g. Pollard and Segall, 1987; Peacock, 2001). Within the Century Mine they are fairly continuous and are found in Proterozoic shales/siltstones, Mesozoic breccia dykes/sills that infiltrate the Proterozoic rocks (Fig. 6.18b), and limestones in the main body of Cambrian rocks (Fig 6.4a, b).

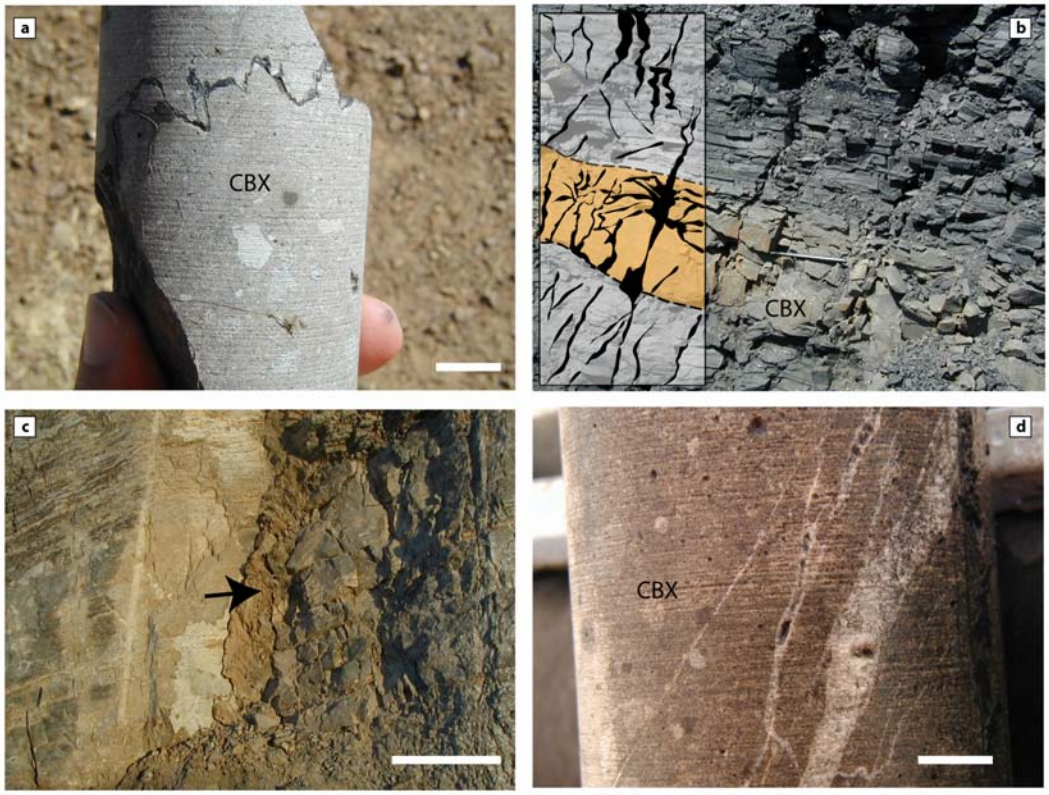

Fig. 6.18 Examples of post-intrusion structural features: (a) compaction related, sub-horizontal, macrostylolite with cuspate, sinusoidal profile (scale bar 1.5 cm). Organic (graphite) solution seams accumulated along the stylolite's margin. The stylolite cuts carbonate breccia (CBX) postdating its emplacement. (b) Image portraying field relationships among joint distribution, a CBX sill, and basement shales/siltstones. Sketch outlines evidence of jointing/fracturing developed across the different lithotypes (pen for scale). (c) Example of joint Type 2 (length >10 m) containing fault gouge material (arrow, scale bar 1.5 m). Fault gouge differs from carbonate breccia infill as it is composed of soft, friable micaceous claystone entraining chips and cm-scale clasts of carbonate limestone. Type 2 joints cross-cut carbonate breccia postdating breccia emplacement, see Fig. 6.12a (moon symbol for location). (d) Example of network of calcite veins cross-cutting CBX breccia (scale bar 1cm).

Two distinct generations of joints were identified in the Century Mine (Type 1 and Type 2). An array of sub-parallel joints intersects both carbonate breccia and shale/siltstone layers in the basement (Fig. 6.18b) and is also widespread across the whole mine, occurring in Cambrian cover. These joints frequently occur in complicated

networks, forming numerous dihedral intersections that originate by combination of steep dipping joints with reactivation of weak, cohesionless bedding planes (Fig. 6.18b). Other joints are distinct because of their more consistent orientation (NW-NNW) and infill (Type 2, see Fig. 6.18c), and because of their scale (exceeding 10's of metres). Specifically, they contain a clay-carbonate rich fault gouge that is interpreted as possible tectonic comminution associated with later post-Cambrian shearing. Type 2 joints have also wider spacing, becoming isolated fractures/faults.

Field observations were complemented with structural mapping of fractures and joints along three transects (eastern wall of the Century Mine, stage 4 – transect 1, RL 1120 m and transect 3, RL 1088 m; western wall of Century Mine, stage 5 – transect 2, RL 1104 m). The fieldwork aimed to outline the influence of pre-existing faulting on the joint/fracture distribution. Two approaches were implemented: (1) stereonet based plotting of structural data; (2) scanlines to quantitatively analyse fracture density variation relative to fault proximity. Three plots summarise the orientations of the data collected (Fig. 6.19a-c). In particular, two rose diagrams are presented showing the orientation of steep dipping joints/fracture sets (dip $\geq 60°$) measured in cover and basement (Fig. 6.19a, b). Three trends (NNE-SSW, E-W, and NW-SE) occur in cover rocks and similarly in basement. NNE-SSW and NW-SE joints persist with similar abundance although there is a slight variation in abundance of E-W joints in spite of more ENE-WSW joints in the basement. NW-SE joints are less abundant compared to the other trends both in cover and basement.

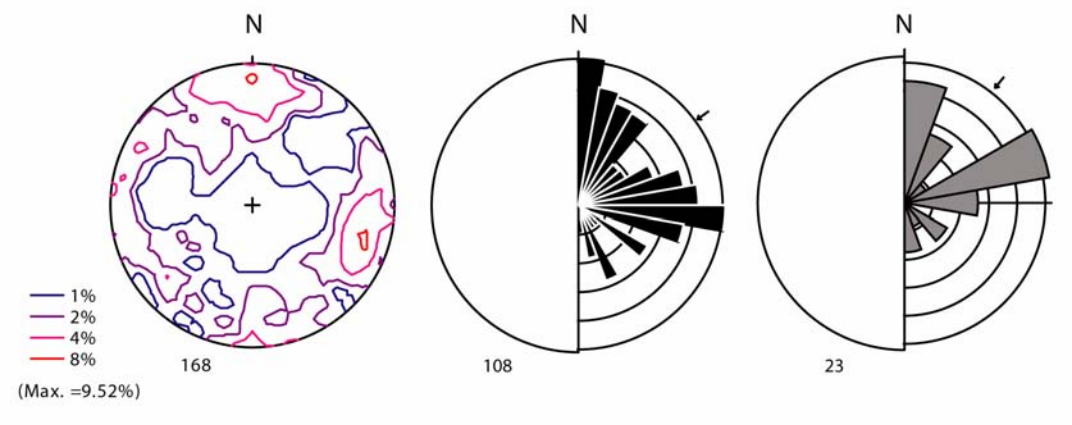

Fig. 6.19 Stereoplots representing the preferential trend of distribution expressed in % area for the whole joint dataset and rose diagrams of joints measurements in Middle Cambrian limestone (black, 15º sector) and Mesoproterozoic shales/siltstones (grey, 20º sector). For comparison see discussion in the text.

Joints in cover were compared with joints in basement to differentiate between structures exclusive of Proterozoic rocks from structures that likely formed both in cover and basement during Palaeozoic time. NNE and NW and E-W striking joint sets have close orientation in basement and cover. Therefore, they formed in a similar stress-field during post-Cambrian tensile failure. The joint set striking ENE is more prominent in the basement, however this may be a) real, b) due to the variation in orientation of selected transects, or c) bias induced by the sample size considering that partitioning of deformation and local influence of pre-existing faults causes inhomogeneous distribution of joints (Hancock, 1985).

To evaluate a possible relationship between joints and older faults, poles to joints are compared with the previous plots of faults and dykes orientations. In general Hancock (1985) remarks that joints tend to be rarely parallel both in strike and dip to

the main plane of dip-slip faults or thrusts. This would favour a more common situation that sees a time gap between faulting and jointing. In the Century Mine a good correlation between the two datasets exists. However, Type 1 joints cut CBX suggesting a time separation between these sets and faulting related to the intrusion of the CBX breccia. Type 1 Joints propagated as planar tensile fractures cross-cutting different rocktypes, suggesting that variation of mechanical properties of the host played minor control on their development (see Engelder, 1985). Therefore, their origin is possibly due to unloading or release, during uplift and erosion (Engelder, 1985). A shallow depth of formation seams a more reasonable solution to explain also the local occurrence of iron oxides-hydroxides (hematite, limonite, goethite) as matrix infill in these joints (e.g. Perez and Boles, 2005). It is likely that some joints formed by reactivation of older faults (Type 2), but others formed later, independently (Type 1). Rather than necessarily requiring reactivation, older basement faults may have only acted passively, because pre-existing anisotropies tend to control the orientation of later tensile fractures/joints (Zhang and Sanderson, 2002).

To further address this issue, image processing of four scanlines was undertaken (along transect 2) to measure the density variation of fractures/joints as a function of distance from a major E-W fault that records Palaeozoic movement. The selected fault (Pandora's Fault, Fig. 6.20) is also intruded by carbonate breccia. In a recent contribution, Peacock (2001) remarks that a possible key distinguishing factor for joints and fractures that form contemporaneously with dip-slip faulting could be their increasing number towards a fault zone (see also Hammond and Evans, 2003).

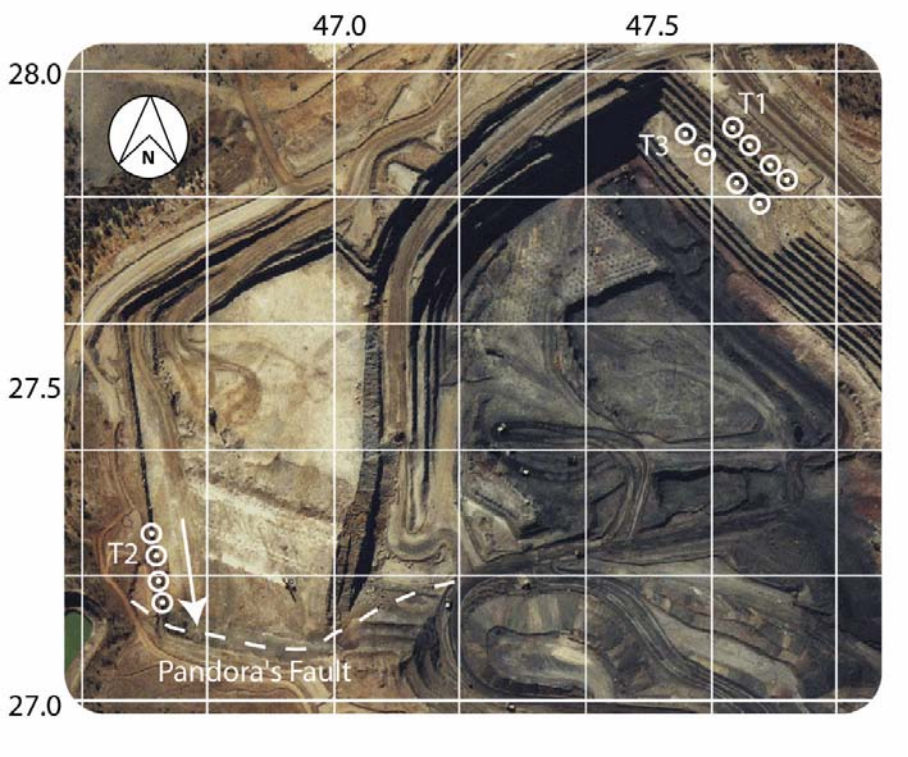

Fig. 6.20 Map-view of the northwestern corner of the Century Mine illustrating transects where structural data were collected (T1-T3). Along T2, photographic sampling of fractures were collected in four locations within a 140 m interval, dashed line indicates approximate location of the Pandora's Fault.

Four scanlines of one metre each were sampled with spacing of approximately 35 metres along the western wall of the Century Mine. This section represented an optimal condition where only joints and fractures were observed along the photographed transect. The scanlines were photographed at equal distance from the limestone exposure (3 m) orthogonal to the pit face to respect the scale dependency factor which conditions the fracture density estimation. Collected images were processed using the MATLAB ® Image Processing Toolbox, which allows: (1) image contrasting, (2) edge detection of linear features (e.g. fractures etc.), and (3) pixel

profiling and counting after threshold and subsequent binary conversion. Fig. 6.21 illustrates four plots representing the density distribution of fractures/joints across each (1 m) scanline and the relative density of edges per column of pixel data. A final plot also considers a comparison of the local (area based) density of fracturing/jointing every 35 m interval.

The density variation measured along the 140 m transect does not appear to be related to the major fault, at least within the constraints of our sample spacing. In contrast with the general observations of some orientational relationships between faults and joints, these data suggest that earlier syn-sedimentary Cambrian faults where not substantially reactivated to produce the later joints. It is therefore more likely that the majority of the joints (Type 1) formed unrelated to faults although in a tectonically preconditioned scenario in which rock's anisotropies contributed to their trends.

The investigation of the timing of fracturing and jointing thus provides only limited constraint on the age of the Lawn Hill Megabreccia. Some of the brittle structures (Type 2) indicate possible tectonic reactivation of the system during post-Cambrian deformation that however was unrelated to the megabreccia event. More likely both types of joints formed during unroofing linked to late-Devonian Alice Springs Orogeny (ca. 410-390 Ma). Twinning fabrics and subgrains development in CBX clasts may be the result of this later tectonic movement, as well as some of the hydrothermal calcite veins observed on the eastern wall of the mine. Alternatively, the hydrothermal calcite-veining and pressure solution seams could be linked to dewatering

and basin compaction at relatively shallow depths, 10's to 100's of metres, soon after formation of the megabreccia (Feltrin et al., 2003; Oliver et al., 2006).

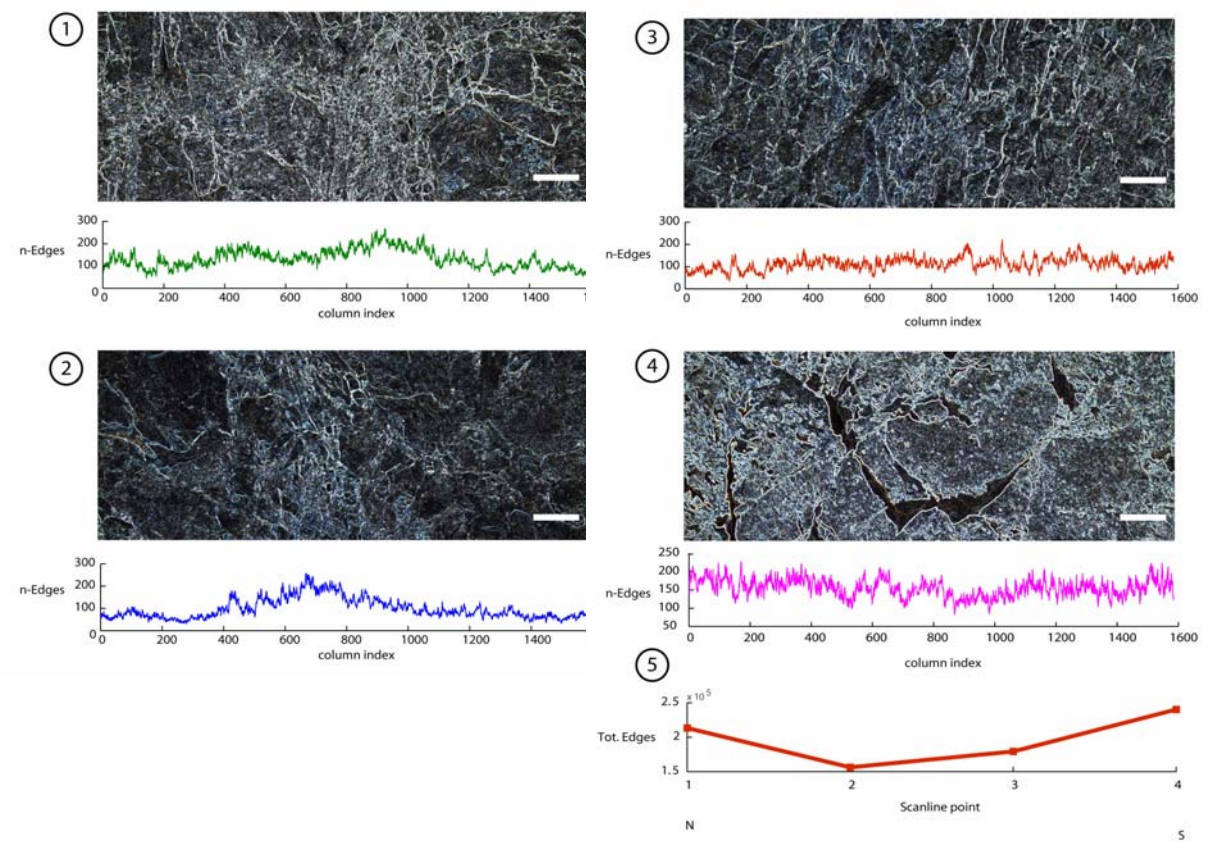

Fig. 6.21 Scanlines along transect 2 ordered from north to south. The density of fracturing has been computed as the number of pixels/edges derived from image processing (edge detection). This approach was utilised to produce binary files used then to plot cumulative slopes representing the total number of edges for each column of the scanline – a parameter that gives a quantitative estimation of the horizontal variation of fracture density across a single scanline (1 to 4). Scanline results were also summed up to get a total number of edges for the whole area and they were compared to obtain an evaluation of the density of fractures/joints variation at larger scale (5).

6.4.4.3 Carbon and oxygen isotope analyses of hydrothermal phases

To allow the characterisation of these hydrothermal events, stable isotope analyses were performed on whole rock and veins (Table 6.2). These include host rock, cements and veins from cover, basement rocks, and also calcite veins intersecting carbonate breccia and basement. Fig. 6.22 schematically shows the spatial relationship of isotopic data to field locations, and also a schematic representation of the rock-types. Petrography was used to refine the otherwise ambiguous interpretation of isotopic data.

Results are presented in the conventional terminology with $\delta^{13}C$ referenced to PDB and $\delta^{18}O$ relative to SMOW. Analyses were performed on powdered carbonate with phosphoric acid (McCrea, 1950; Swart et al., 1991), and using the mass spectrometer of the Central Science Laboratory of the University of Tasmania.

The results were (1) thirteen analyses comprising whole rock (carbonate) and calcite-veins of Mesozoic age (Thorntonia Limestones) with $\delta^{13}C_{carb}$ ranging from -14.8 to 0.8 $^{0}/_{00}$ with average -3.1 $^{0}/_{00}$, and $\delta^{18}O_{carb}$ 9.9 to 23.9 $^{0}/_{00}$ with average 20.9 $^{0}/_{00}$ in average; (2) four carbon isotopic values on organic matter (pyrobitumen) found in stylolites occurring in mottled limestone in the cover (CLS55), and shales from the basement (SH75, SH23, SH12), with values within the interval -27.8 to -33.5 $^{0}/_{00}$ $\delta^{13}C_{graph}$, mean -30.1 $^{0}/_{00}$; and (3) three siderite veins in Proterozoic basement ranging from -5.2 to -4.3 $^{0}/_{00}$ $\delta^{13}C_{carb}$ averaging -4.8 $^{0}/_{00}$, and 15.8 to 16.8 $^{0}/_{00}$ $\delta^{18}O_{carb}$ averaging 16.6 $^{0}/_{00}$. All data are reported for convenience in Table 6.2 and separated in groups (whole rocks, veins, etc., see also Fig. 6.22), according to the following discussion.

Table 6.2. Carbon and oxygen isotope analyses of whole rock and veins on the Thorntonia Limestone and Mesoproterozoic basement hosting carbonate breccia dikes (Century area).

Sample Name	*Transducer*	*Delta 13C*	*Precision*	*Delta 18O*	*Precision*	*Delta 18O*	*Description*
(alternate)	*(mBar)*	*wrt PDB*	*Delta 13C*	*wrt PDB*	*Delta 18O*	*wrt SMOW*	
C-63-R	*30.2*	*0.5*	*0.011*	*-6.7*	*0.009*	*23.9*	*Marl*
C-69	*16*	*0.1*	*0.012*	*-7.8*	*0.007*	*22.8*	*Carbonate breccia*
C-65	*20.4*	*0.2*	*0.007*	*-6.7*	*0.013*	*23.9*	*Nodular phosphatic bedded limestone*
C-62	*27.4*	*0.7*	*0.011*	*-8.9*	*0.015*	*21.7*	*Mottled cherty limestone (siliceous nodules)*
C-64	*22.2*	*0.6*	*0.01*	*-8.9*	*0.015*	*21.7*	*Fenestral dolomite*
C-6	*0*	*0.4*	*0.012*	*-8.8*	*0.009*	*21.8*	*Stylolitic limestone*
C-7	*22.2*	*0.4*	*0.01*	*-8.9*	*0.008*	*21.7*	*Dolomitic limestone*
C-43-V-BCS	*15.5*	*-8.3*	*0.008*	*-9.1*	*0.013*	*21.5*	*Calcite vein in Mesoproterozoic (shale)*
C-74-V	*15*	*-10.4*	*0.014*	*-9.3*	*0.016*	*21.3*	*Calcite vein in Mesoproterozoic (siltstone)*
C-9-V	*20.7*	*-1.4*	*0.014*	*-10.5*	*0.012*	*20.1*	*Calcite vein in dark, grey, stylolitic and phosphatic limestone*
C-54-V	*0*	*-14.8*	*0.006*	*-20.3*	*0.01*	*9.9*	*Calcite vein in mottled limestone*
C-63-V	*15*	*0.8*	*0.009*	*-10.9*	*0.006*	*19.6*	*Calcite vein in marl*
C-43-V-CBX	*19.2*	*-9.0*	*0.013*	*-9.4*	*0.016*	*21.2*	*Calcite vein in dolomitic breccia*
SH75	*0*	*-33.4*	*0.013*				*Nodule of siderite in shale Mesoprot. (sample C-291 G. Broadbent collection)*
CLS55	*0*	*-29.6*	*0.005*				*Organic-rich stylolites in mottled Cambrian limestone*
SH23	*0*	*-29.7*	*0.019*				*Hydrocarbon in fractures - Mesoproterozoic siltstones*
SH12	*0*	*-27.8*	*0.008*				*Mesoproterozoic shale*
C-41-V	*0*	*-4.3*	*0.015*	*-13.6*	*0.007*	*16.8*	*Siderite vein - Mesoproterozoic*
C-46-S	*0*	*-5.2*	*0.008*	*-14.6*	*0.005*	*15.8*	*Siderite vein - Mesoproterozoic*
C-46-H	*0*	*-5.0*	*0.005*	*-14.5*	*0.012*	*15.9*	*Siderite vein - Mesoproterozoic*

Whole rock isotopic signatures from Century Cambrian limestones are in general agreement with global Lower/Middle Cambrian boundary data (Brasier and Sukhov, 1998; Veizer et al., 1999; 2000) obtained from brachiopods from the Amgan Stage, northern Siberia. The Century data obtained for Middle-Cambrian limestone also have isotopic signatures similar to the ones reported by Lindsay et al. (2005) in Thorntonia Limestone outcropping within the O'Shannassy River, 9 Km south of Riversleigh Homestead, in the northeastern part of the Georgina Basin. These workers report slight depletions in $\delta^{13}C_{carb}$ and $\delta^{18}O_{carb}$ relative to normal Cambrian marine seawater signatures, probably due to diagenetic recrystallisation and fluid flow in the more permeable grainstone units of the Thorntonia Limestones. Results from whole rocks at Century reflect a similar trend with approximately a 2 $^{0}/_{00}$ $\delta^{18}O_{carb}$ difference between fresh and isotopically lighter, dolomitised limestones.

The carbonate breccia has values indistinguishable form the limestones. Analysed veins show similar $\delta^{18}O_{carb}$ isotopic trends, but oscillations are shown for $\delta^{13}C_{carb}$ and $\delta^{18}O_{carb}$ in veins sampled in limestones, suggesting some degree of open system behaviour during veining (Bons, 2001; Oliver, 2001), possibly linked to meteoric input (Faure, 1991; Aranburu et al., 2002) or diagenesis, because $\delta^{18}O_{carb}$ values are comparable with dolomites and diagenetically altered limestones. Slight depletion in $\delta^{13}C_{carb}$ for some veins may suggest that the system interacted with other carbon rich reservoirs (organic-rich basement shales or petroleum reservoirs hosted in limestones) that are strongly depleted in $\delta^{13}C_{carb}$ (mean of -30.1 $^{0}/_{00}$ $\delta^{13}C_{graph}$). A marked depletion in $\delta^{13}C_{carb}$ observed in a calcite vein cross-cutting carbonate breccia and basement shale along a fault contact is indicative of a possible basement interaction.

Similar trends are observed for veins crosscutting the breccia and basement, which are also strongly depleted in ^{13}C (mean, -9.3 $^{0}/_{00}$ $\delta^{13}C_{carb}$). A single sub-horizontal vein in mottled limestone, which was part of a pressure solution related network of veins, shows even more marked depletion in $\delta^{13}C_{carb}$ and $\delta^{18}O_{carb}$ (see, Table 6.2). This "anomalous value" may be linked to proximal petroleum sources hosted in cover rocks in the Middle-Cambrian limestones. Bitumen was observed in stylolite seams and cavities in porous sandy-limestone on the northern exposure of the Century Mine.

Siderite veins sampled on the northeastern corner of the Century deposit, where the basement abuts against cover, revealed signatures comparable to the data reported by Broadbent et al. (1998) suggesting an earlier origin linked to the Proterozoic mineral deposit and other smaller regional occurrences; therefore, they are considered unrelated to the Mesozoic calcite veining event.

In summary, the similarity of data for breccia and limestone suggests that lithification of both rocks occurred at similar depths (temperatures) from similar sources, and similar fluid involvement. These all suggest that the breccias lithified at shallow depths. $\delta^{18}O_{carb}$ values in veins likely represent the mixing of seawater carbonate dominated signatures with a meteoric component, or reflect late diagenetic recrystallisation in response to pressure solution at slightly elevated temperatures. The evidence of calcite veins with characteristic depletion in ^{13}C along breccia/fault boundaries across basement contacts suggests that faults were involved with fluid flow across the cover/basement interface during the burial history.

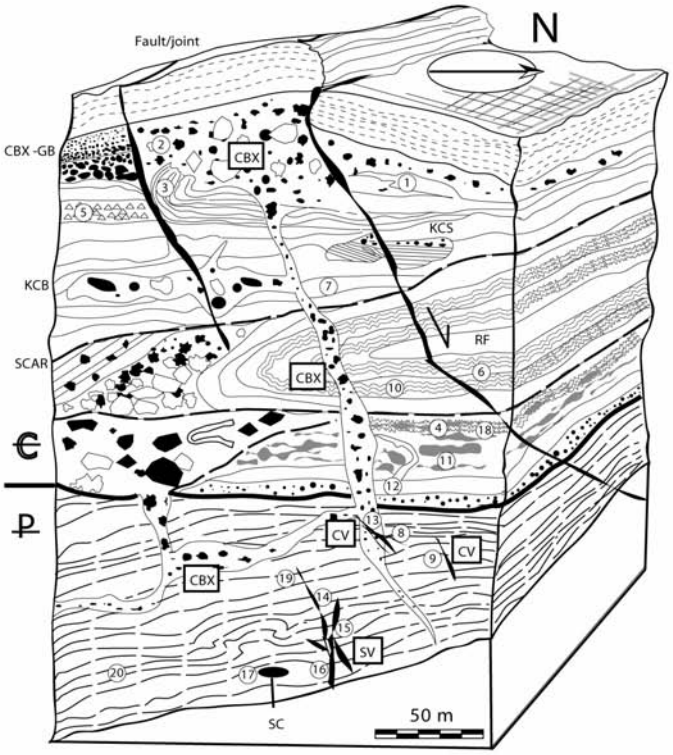
Fault/joint
N
CBX -GB
KCB
SCAR
CBX
KCS
RF
CV
SV
SC
50 m

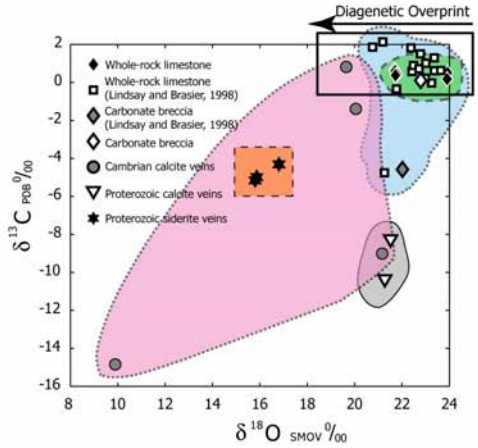
Diagenetic Overprint
Whole-rock limestone
Whole-rock limestone (Lindsay and Brasier, 1998)
Carbonate breccia (Lindsay and Brasier, 1998)
Carbonate breccia
Cambrian calcite veins
Proterozoic calcite veins
Proterozoic siderite veins
δ13C PDB 0/00
δ18O SMOV 0/00

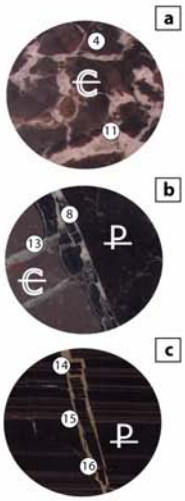
a
b
c

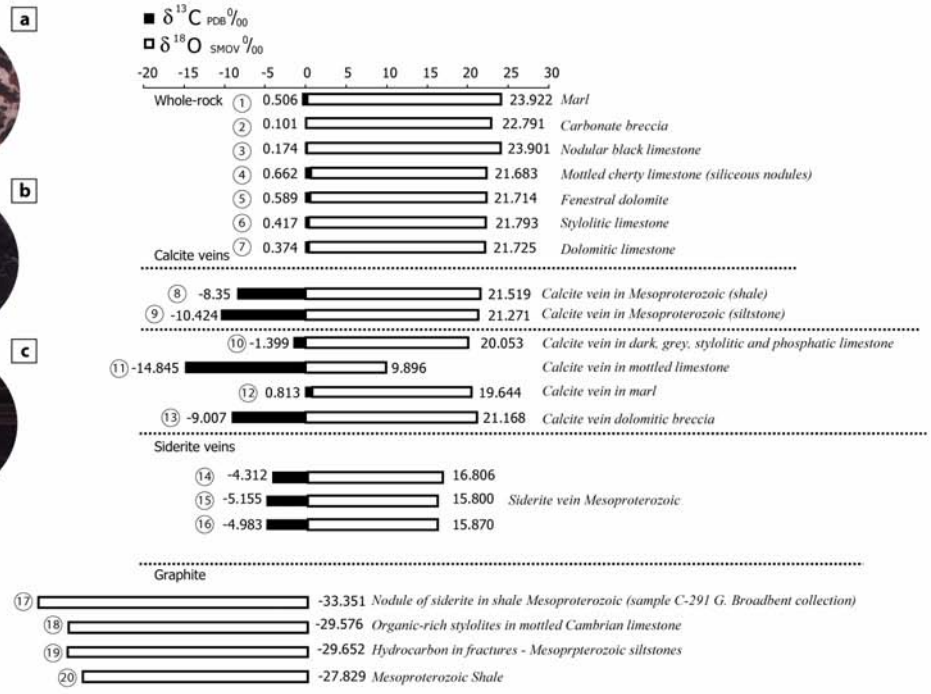
δ13C PDB 0/00
δ18O SMOV 0/00
Whole-rock
Calcite veins
Siderite veins
Graphite
1 0.506 23.922 Marl
2 0.101 22.791 Carbonate breccia
3 0.174 23.901 Nodular black limestone
4 0.662 21.683 Mottled cherty limestone (siliceous nodules)
5 0.589 21.714 Fenestral dolomite
6 0.417 21.793 Stylolitic limestone
7 0.374 21.725 Dolomitic limestone
8 -8.35 21.519 Calcite vein in Mesoproterozoic (shale)
9 -10.424 21.271 Calcite vein in Mesoproterozoic (siltstone)
10 -1.399 20.053 Calcite vein in dark, grey, stylolitic and phosphatic limestone
11 -14.845 9.896 Calcite vein in mottled limestone
12 0.813 19.644 Calcite vein in marl
13 -9.007 21.168 Calcite vein dolomitic breccia
14 -4.312 16.806
15 -5.155 15.800 Siderite vein Mesoproterozoic
16 -4.983 15.870
17 -33.351 Nodule of siderite in shale Mesoproterozoic (sample C-291 G. Broadbent collection)
18 -29.576 Organic-rich stylolites in mottled Cambrian limestone
19 -29.652 Hydrocarbon in fractures - Mesoprpterozoic siltstones
20 -27.829 Mesoproterozoic Shale

Fig. 6.22 3D Block diagram representing a summary of the field relationships discussed in the text and presented in previous plates. (GB) graded breccia, (KCS) karst cavity containing sandstone fill; (KCB) Karst cavity with breccia fill; (CBX) carbonate breccia dyke; (CBX-GB) carbonate breccia with normal grading; (CV) calcite vein; (SV) siderite vein; (SC) siderite concretion. Location of specimens where carbon and oxygen isotopic ratios were measured is given within the portrayed spatial context (see numbering 1-20) and relative reference to the histogram and scatter plot. Three examples of photographed veins are also documented representing, calcite veins in cover, calcite veins cross-cutting cover and basement, and siderite veins in basement (a, b, c).

6.5 Discussion and conclusions

A summary of the documented spatial and temporal constraints is presented to ascertain the timing of failure and consequent megabreccia development in the Lawn Hill Outlier. Finally, the geological, causative agents are assessed – seawater eustatic variations, earthquake or meteorite impact?

6.5.1 Timing of the megabreccia

6.5.1.1 Importance of the tectonostratigraphic reconstruction

There is a ~100 m.y. gap between Middle-Cambrian sedimentation and later orogenic inversion of the Georgina Basin (Alice Springs Orogeny). Bedded limestones, outcropping in the Lawn Hill Outlier, were thus sedimented during subsidence in an overall extensional setting. This orogen has likely controlled the later Devonian sedimentary evolution, and at least part of the deformational features occurring in the

whole stratigraphic sequence. However, the style of folding of the Thorntonia Limestone supports its early synsedimentary origin. More likely, the folds developed on a palaeoslope dipping toward SE, and were driven by extensional deformation unrelated to the Alice Springs Orogeny. This latter interpretation is corroborated by the 3D reconstruction and quantitative estimation of dyke trends in basement. The dikes formed preferentially along NW to WNW faults suggesting that they may have developed contemporaneously with the slumping. The deformation likely caused reactivation of NW and WNW structures because they were more prone to dip-slip reactivation (Sibson, 1985). These scenarios could be explained by a steepened ramp/slope and fault induced destabilisation contributing to the Lawn Hill Megabreccia formation.

6.5.1.2 Paragenesis of deformational features

The structural style of folding is only one of several features suggesting an early origin for the megabreccia. The paragenetic reconstruction based on cross-cutting relationships (Fig. 6.23) suggests that a component of the Lawn Hill Megabreccia (CBX) formed initially as sedimentary breccia (derived from mass-flow and also debris and turbidites), but then the destabilisation of the platform caused reorganisation of this breccia-type causing the formation of chaotic structures including dykes that infiltrated the basement. MB is similarly derived from such destabilisation process that however involved the marl lithofacies rather than the CBX. In this context, the relationship among CBX and MB indicates that recumbent folding was at least initially synchronous

with CBX and MB formation. Superposed on these deformational phases the action of fluids penetrating the ramp margin may have favoured destabilisation, because the meteoric and/or seawater flows were able to dissolve the limestone forming SB and relative cavities that resulted in local collapse filled by CBX and in situ breccias CB. This process was contemporaneous with CBX redistribution but may also have predated the CBX phase. The occurrence of stylolites in CBX dykes is a plausible indication that the breccia was intruded earlier than the Alice Springs Orogeny that more likely was responsible for the two generations of joints observed. The veins observed in a faulted CBX dyke indicates that a calcite-precipitating hydrothermal phase occurred at a depth ranging from few 100's of metres to a few kilometres and that fluid flow occurred between basement and cover. The constraints obtained from Carbon and Oxygen isotope results are insufficient to attribute with certainty these veins to the Alice Springs related reactivation. However, the stable isotopic results confirm the conclusions derived from the style of deformation and cross-cutting relationships, indicating that cementation of CBX dikes occurred early in a relatively seawater-dominated setting (relatively low-temperatures). In summary paragenetic relationships and stable isotopic data suggest an early timing for the Lawn Hill Megabreccia.

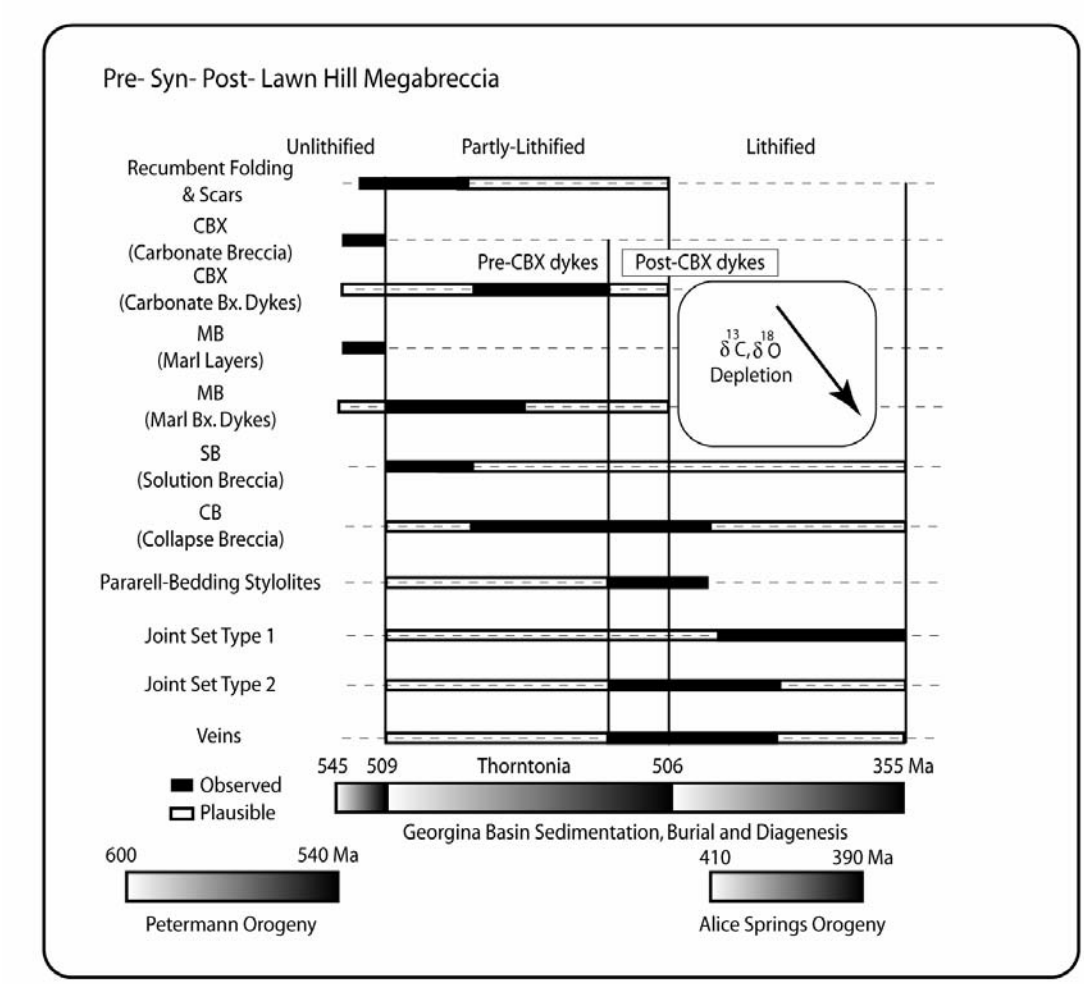

Fig. 6.23 Paragenetic reconstruction of the cross-cutting relationships used to reconstruct the temporal evolution of the sedimentary and tectonic events that contributed to the formation of the Lawn Hill Megabreccia. The diagram includes the early phases of breccia development followed by post-breccia events. The basin evolution led to a gradual depletion in both $\delta^{18}O$ and $\delta^{13}C$ (see text for discussion).

6.5.1.3 Palaeogeographic scenario

A reasonable palaeogeographic scenario is one in which the Thorntonia limestones formed in a shallow epicontinental sea around a topographic high, centred approximately 10 km northeast of the Century Mine. The occurrence of an internal ring of phosphatic limestones in the central part of the small circular platform, could be linked to possible ocean upwelling during sedimentation, governed by this palaeogeographic setting (De Keyser and Cook, 1972; De Keyser, 1973). For instance, Hallock et al. (1988) and Pomar et al. (2002) propose that topography-induced upwelling brings nutrient-rich cold waters to the shelf edge and produces an area of high organic production. This could explain the elevated phosphatic contents in these limestones.

The lithofacies assemblage forming the Lawn Hill Megabreccia more likely formed in a slope setting located seaward of a ramp environment (Fig. 6.24). Mass-flows, debris-flows and turbidites occurring in the Century Mine represent assemblages of these various sedimentary components. The lithofacies variation was a function of the ramp location and comprised barrier-bank complexes of skeletal carbonate, lagoonal carbonates, tidal flats, and supratidal sequences (Fig. 6.24). Lithofacies distinctive of barrier-bank complexes are evaporites, cherts and fenestral dolomites. Notice that these types of ramp have relatively low-angles (usually 1° to 15°) and most likely would be relatively stable. However, sedimentary ramps can evolve to steeper angles in case of fault movement along their margin, as discussed in Payros et al. (1999).

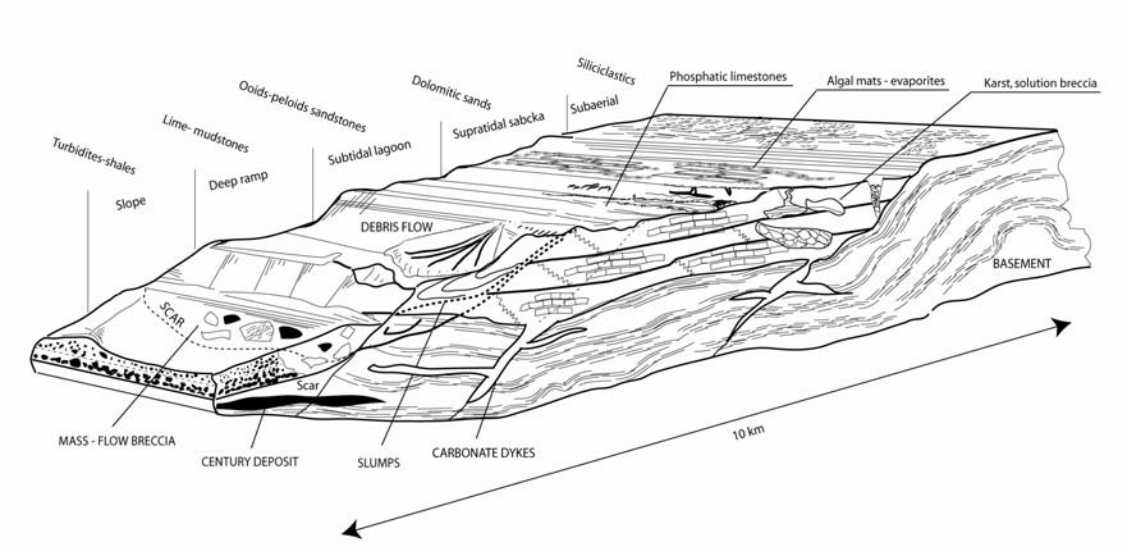

Fig. 6.24 3D Block diagram illustrating the variation of depositional environments across the Lawn Hill Outlier. The reconstruction is based on documented field relationships and lithostratigraphic interpretations of Szulc (1992) and palaeogeographic models proposed by Read (1985). Limestone exposure in the area proximal to the Century Mine is interpreted as part of a slope setting during Middle Cambrian times adjoined to a ramp of barrier-bank type. Recognised styles of brecciation find a logical collocation within this paleoenviromental setting. The 3D diagram illustrates also a possible influence of reactivation of basement structures controlling local steepening of the basinal slope. Superposition of a carbonate platform on a basement high produced by an asteroid impact may have also conditioned the ramp inclination allowing slumping within intertital and subtidal settings.

A contributing component to basal slip along the slope could have been also the localised, intrastratal occurrence of evaporites and dolomites (Fig. 6.8) that may have lubricated and weakened the marginal part of the ramp. For example, Aranburu et al. (2002) describe a close link between dissolution/precipitation processes (karstification) and the Valnero-Ruahermosa fault in the Jorrios Platform of the Basque-Cantabrian Basin, suggesting that a close interrelationship between meteoric circulation of fluids and limestone dissolution along the fault zone were likely to have occurred. As seen the variety of breccias identified in this study emphasise, in conjunction with observed

cavity fills, that karstic dissolution was also prominent in proximity of the Termite Range Fault zone.

6.5.2 Origin of the Lawn Hill Megabreccia - is it the result of an astobleme impact?

As discussed above, the timing of the Lawn Hill Megabreccia and dykes formation appears to be fairly constrained in an early synsedimentary phase, and as seen the synergy of several processes contributed to its formation. However, the data collected and relative interpretations allow only a partial discrimination of the causative agents. In this section three factors are considered: (1) the effect of eustatic variations; (2) the tectonic control; and (3) a meteorite impact.

Eustatic variations can be a prominent destabilising factor along a platform margin. Abrupt pore pressure decreases associated with the fall of eustatic sea-level may lead to drastic increase of differential stresses (Secor, 1965). However, steep inclination of the ramp is a requirement for such model, and therefore other mechanisms have to be invoked to explain the Lawn Hill event. The relative palaeogeographic location in respect to the Georgina Basin and the occurrence of CBX dykes in basement with trends suggesting reactivation of pre-existing basement faults is indicative of a possible extensional, tectonic component. However, another external process may have been contributing to the Lawn Hill Megabreccia formation - an asteroid impact.

Stewart and Mitchell (1987) define some important points regarding the Lawn Hill circular structure (firstly reported by Stewart, 1986) and its possible derivation from a Proterozoic cryptoexplosion - here briefly reviewed: (1) Shock deformation induced mosaic structures observed in quartz grains from shattered fragments (the existence of cone in cone structures is confirmed in this study, Fig. 6.25). Multiple intersecting sets of lamellae indicates impact pressures higher than 10 GPa for the central part of the Lawn Hill Outlier (Officer and Carter, 1991). However, at this location the Mesoproterozoic basement of the Upper Lawn Hill Formation is outcropping (see map in Fig. 6.1c). In fact, no shock deformation microstructures are visible in thin sections of chert breccia sampled in limestone. Additionally, the chert breccia is also found in other localities of the Georgina Basin suggesting that as mentioned previously part of the brecciation formed by solution collapse (Wilson and Hutton, 1980) and debris-flows. (2) “pahoehoe-like” melted rocks were observed at the centre of the inferred crater. (3) The broken folds in the breccia hardly resemble a syn- to post-Middle Cambrian impact. (4) The haphazard nature of the bedding in limestone further supports the hypothesis of a solution collapse.

These arguments were used to suggest that an asteroid impact took place before limestone sedimentation - which is in agreement with the above mentioned phosphate ring formed around the central basement high (Gum Hole Plain). Stewart and Mitchell (1987) remark also that the absence of signs of impact in the surrounding limestones might be the due to their relative distance from the impact site. Moreover a possible explanation for the absence of shatter cones in the Thorntonia Limestone would be a Middle-Cambrian synsedimentary impact - the lack of impact signs could be

consequence of the state of consolidation of the sediments. Shoemaker (1992) pointed out that the size and height of the central uplift are anomalously low compared to other impact structures. However, the topography may have been remodelled by later erosional processes soon after impact and Dypvik and Jansa (2003) suggest that in a submarine impact the crater morphology is generally devoid of well developed rims and also sedimentary processes inside and outside the crater can be variable, causing its reshaping.

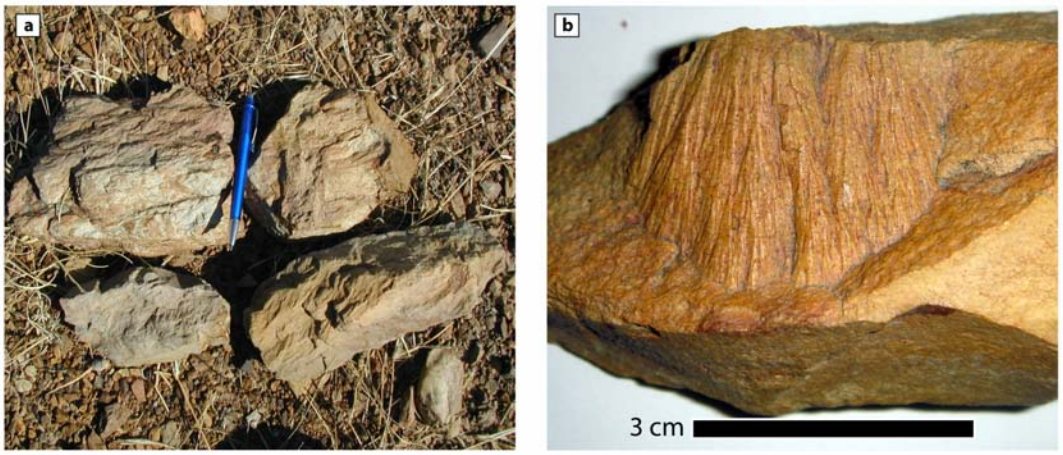

Fig. 6.25 Examples of shatter cones collected in the Gum Hole Plain. (a) Samples of shatter cones found in oxidised siltstones of the Upper Lawn Hill Formation. (b) Enlargement illustrating typical horsetail structure in quartz sandstone (Termite Range Formation). Shatter cones can be formed also in dyke intrusions and volcanic explosions, however if quartz grains display crossed lamellae (in thin section) due to impact they indicate pressure ranges that can be produced only by cryptoexplosion (Stewart and Mitchell, 1987; Shoemaker and Shoemaker, 1996).

A synsedimentary impact represents an attractive alternative to catastrophic gravity driven deposits associated with earthquakes (or tsunami). Dypvik and Jansa (2003) remark that admixtures of melted particles in these deposits (possibly

anomalously enriched in Iridium) would be a distinctive parameter. In this regard Shoemaker (1992) reports limited Iridium contents for suevite sampled in the Lawn Hill crater although this author suggests that the degree of contamination of melted materials can be variable and therefore a cryptoexplosion derivation is often hard to ascertain on this ground. A more recent contribution of Lindsay and Brasier (1998), which adds new carbon oxygen isotopic data on Middle-Cambrian limestones (see Fig. 6.22) led these workers to conclude that the impact predated the limestones deposition, as suggested by Stewart and Mitchell (1987), and Shoemaker and Shoemaker (1996).

Isotopic signatures reported by Lindsay and Brasier (1998) are similar to those presented here on carbonate breccia. The carbonate breccia sampled by Lindsay and Brasier (1998) in the northern part of the annular structure also revealed values similar to the sedimentary limestones confirming that these rocks and the breccia lithified after the meteorite impact and are normal marine carbonates. Lindsay and Brasier (1998) consider seawater derived, isotopic signatures a distinctive parameter as markedly lighter values would result from melting of carbonates after an impact. However, the lack of anomalous isotopic signatures may have been a function of distance from the main site of impact. Also in the case of sub-marine impact the isotopic signature would be more likely seawater dominated if the sediments were not yet lithified.

Further investigations, on the Iridium content in limestones might be a possible way to ascertain a Middle Cambrian impact provided that evidence of melted fragments can be ascertained. However, the evidence of shock induced, intersecting micro-lamellae in quartz crystals represents a strong indication that a cryptoexplosion did occur in the Lawn Hill Outlier. What remains uncertain is the timing of this event and

therefore its possible connection to the Lawn Hill Megabreccia. Multiple depositional/erosional scars provide an indication that the megabreccia, more likely, originated from a sedimentary process (multiple debris-flows and turbidites). The data are however insufficient to completely discount the direct involvement of a sub-marine impact.